# Biogeochemistry in an intertidal pocket beach

Aurélia Mouret, Céline Charbonnier, Pascal Lecroart, Édouard Metzger, Hélène Howa, Bruno Deflandre, Loris Deirmendjian, Pierre Anschutz

# BIOGEOCHEMISTRY IN AN INTERTIDAL POCKET BEACH

Aurélia Mouret[1], Céline Charbonnier[2], Pascal Lecroart[2], Edouard Metzger[1], Hélène Howa[1], Bruno Deflandre[2], Loris Deirmendjian[2,3], Pierre Anschutz[2*]

[1] UMR CNRS 6112, LPG-BIAF, Univ. Angers, Univ. Nantes, F-49045 Angers Cedex, France

[2] Université de Bordeaux, CNRS, EPOC, UMR 5805, F-33400 Talence, France

[3] Present address : Géosciences Environnement Toulouse (Université de Toulouse, CNRS, IRD, UPS), Observatoire Midi Pyrénées, Toulouse, France

* Corresponding author: pierre.anschutz@u-bordeaux.fr

## Abstract

Sandy beaches are places of active organic matter mineralization due to water renewal providing organic matter and electron acceptors in the porous and permeable sands. Recycled biogenic compounds are efficiently transferred to the coastal marine environment via wave and tidal-driven advective flows. The biogeochemical processes in beach aquifers were mainly studied in semi enclosed systems with low tidal amplitude, and with a connection to continental aquifers contributing to solute fluxes to the coast from terrestrial groundwater. We present here the study of a pocket beach isolated from terrestrial aquifers with a high tidal amplitude and a medium energy wave regime. In situ measurements, cross-shore profiles and vertical sampling were conducted during several tidal cycles in spring and autumn. Cross-shore transects, obtained at low tide from holes that represent a mixture of the upper 20 cm of the water saturated zone, showed concentration gradients of redox and recycled compounds. Increase in $pCO_2$, dissolved phosphate and ammonium concentrations downslope revealed that more products from organic matter mineralization accumulated in the lower beach. The related increase in total alkalinity downslope indicated that the part of anaerobic processes in organic matter oxidation was higher in the lower beach. Concentration and $\delta^{13}C$ of dissolved inorganic carbon in pore waters suggested that the carbon mineralized in pore waters came from marine plant debris that were mixed with the sand. Continuous probe records of dissolved oxygen saturation and vertical profiles revealed a tidally-driven dynamics of pore water in the first centimetres of the lower beach aquifer. Ventilation of pore waters corresponded to wave pumping and swash-induced infiltration of seawater in the upper 10–20 cm of sediment. Nutrients and reduced compounds produced through organic matter mineralization remained stored in pore water below the layer disturbed by wave. The flux of these components to seawater is possible when this interface is eroded, for example when wave energy increases after a less energetic period. The low extension of the studied aquifer, typical of pocket

beaches, limits the connection with continental groundwater. Both tidally-driven and wave-driven recirculation of seawater allows pocket beaches to be efficient bioreactors for marine organic matter mineralization. As such, they provide the coastal environment with recycled nutrients, and not new nutrients.

Keywords: Submarine groundwater discharge; beach aquifer; nutrients; carbon cycle; Yeu island

## 1. Introduction

Almost one third of the world's ice-free shoreline is sandy (Luijendijk et al., 2018). Sandy beach sediments are permeable and constitute unconfined aquifers where pore water can circulate. Both terrestrial and marine forces drive underground water flows within beach sedimentary bodies. Resulting submarine groundwater discharge (SGD) can be a significant source of dissolved ions, nutrients, or contaminants to the coastal ocean (Sawyer et al., 2016; Slomp and Van Cappellen, 2004). Marine forces such as tidal pumping and wave-induced pressure gradients may induce fluid flow into superficial permeable sediments (Ataie-ashtiani et al., 2001; Burnett et al., 2003; Moore and Wilson, 2005). Along tidal coasts, seawater circulating through intertidal sandy beach sediments can contribute to 90% or more of SGD and its associated geochemical signature (Li et al., 1999). Hence, intertidal sandy beaches are the place of a large recirculation of seawater.

Sandy beaches generally have low sedimentary organic matter content (Boudreau et al., 2001). However, numerous studies have shown that they are very active places of remineralization due to water renewal in the porous and permeable media providing organic matter and electron acceptors, mostly oxygen from seawater (Anschutz et al., 2009; Billerbeck et al., 2006; Charbonnier et al., 2013; Rocha et al., 2009; Santoro, 2010). When remineralization products are discharged into the coastal ocean via recirculation of seawater, they eventually stimulate primary production and may even cause harmful algae blooms and eutrophication on the inner shelf (Paerl, 1997).

Terrestrial hydraulic gradients result in a net fresh water input into the ocean when terrestrial groundwater mixes with recirculating seawater. The transition between saline pore water and fresh groundwater is called subterranean estuary (Li et al., 1999; Moore, 1999). The sharp interface between water masses of distinct salinities may represent a redox front, which has the potential to reduce nutrient and contaminant loading via groundwater through removal processes such as denitrification and phosphate sorption onto mineral surfaces (Charette and Sholkovitz, 2002; Kroeger and Charette, 2008; Slomp and Van Cappellen, 2004; Spiteri et al., 2006).

Beach hydrology and biogeochemistry response to groundwater, tidal, and wave forcing have been extensively studied. Most of the field studies were conducted on relatively protected beaches characterized by micro- (< 2m range) or meso-tidal regimes (2 to 4 m range), such as Waquoit Bay in the western Cape Cod (Abarca et al., 2013; Gonneea and Charette, 2014), Cape Henlopen at the outlet of the Delaware Bay (Hays and Ullman, 2007; Ullman et al., 2003), Magdalen Island (Couturier et al., 2017), Long Island sound (Tamborski et al., 2017), Tolo Harbour, Hong Kong (Liu et al., 2018) and Ria Formosa (Rocha et al., 2009). The low-energy conditions occurring along these beaches allowed scientists to deploy fragile sampling devices such as wells and in-situ monitoring probes. In agreement with hydrological models tested with similar low hydrodynamic conditions (e.g., Boudafel, 2000; Robinson et al., 2007), most of the aforesaid studies showed that a beach aquifer was often characterized by a sharp transition zone between saline water and fresh water. This interface has a steep slope and is generally located close to the low tide level. Infiltration of saline water into the fresh groundwater in the tidal zone creates a reactive intertidal recirculation cell (Austin and Masselink, 2006; Turner and Masselink, 1998; Bratton, 2010) that has been referred to as the upper saline plume (e.g., Brovelli et al., 2007; Robinson et al., 2006; Santos et al., 2009; Vandenbohede and Lebbe, 2006). The magnitude of the tidal circulation cell and the associated transport of solutes within the beach aquifer increase with higher tidal range, steeper beach slope and hydraulic conductivity as well as lower in-land hydraulic gradient (Li et al., 2009; Robinson et al., 2007). The highly transient nature of the intertidal circulation cell over neap tide-spring tide and seasonal time scales has been evidenced on a micro-tidal beach system (Heiss and Michael, 2014). Studies were also carried out on high-energy beaches shaped by both a high mean tidal range and a high wave exposure, such as the Truc Vert beach on the French Atlantic coast (Anschutz et al., 2009) or the Spiekeroog Island off the North-West German coastline (Beck et al., 2017). In such hydrodynamic context, seasonal erosion and accretion processes drastically reshape the beach profile (Castelle et al., 2014). The unconfined aquifer of the intertidal zone generally consists of saline waters, the intertidal salt water plume being deeper than in low-energy beaches. In the upper meters of the intertidal aquifer, water has a short residence time due to the combined effect of efficient tidally driven recirculation of saline pore water and high permeability of sands (e.g. Charbonnier et al., 2013). Circulation of saline pore water may drag parcels of brackish waters from meteoritic groundwater mixture that may seep out the aquifer at the lower beach level (Buquet et al., 2016), contributing to the flux of nutrients to the ocean (Anschutz et al., 2016).

Small pocket beaches are common worldwide along rocky shorelines (Short and Masselink, 1999). Undergoing limited sediment supply, pocket beaches present generally thin thickness of sand deposited in the intertidal zone above the underlying bedrocks. Thus, the fresh water aquifers connected to pocket beaches are generally restricted, making the offshore fresh groundwater

discharge very weak. Consequently, pore water in tidal pocket beaches mainly consists of recirculating seawater. Here, the purely marine dimension of the biogeochemical reactor that a beach represents can be studied, with associated features and implications such as benthic-pelagic coupling and organic carbon respiration. To our knowledge, documentation on pocket beach pore water circulation coupled to biogeochemical processes is scarce, even missing in case of pocket beach with high tidal range.

In this paper, we report observations on a high tidal range pocket beach located on the Yeu Island off the French Atlantic coast to investigate short-term (tidal scale) dynamics of biogeochemical compounds in pore waters at two contrasted seasons (spring and autumn) by way of detailed cross-shore, and vertical characterization of biogeochemical compounds in the sandy beach aquifer. Two field campaigns were then conducted during periods of contrasted beach morphology, in October 2012 and April 2013. In October the beach displays the highest volume of sand stored in the intertidal area during summer good weather accretion, whereas in April the beach is highly eroded after winter storms. During each campaign, cross-shore profiles allowed to describe biogeochemical processes from the upper to the lower beach. Vertical profiles obtained in the sandy beach aquifer from home-made vertical sampling collectors enabled to collect pore waters at several depths and at different time after the tidal emersion. Finally, *in-situ* probes were buried in sediments to describe the dynamics of dissolved $O_2$ during several consecutive tidal cycles.

## 2. Material and methods

### *2.1. Study area*

Located in the Bay of Biscay, Yeu Island is 8 km long and 3 km wide, elongated in a NW-SE direction about 20 km off French Atlantic coast (Fig. 1). The orthogneiss substrate of the island is gently sloping from erosional cliffs along the southern coast that reaches 32 m at its highest point, to nearshore bedrock outcropping at 0 to -2 m along the north-eastern coast (Durand et al., 2014). This NE coast consists of a succession of sandy pocket beaches partitioned by hard rock headlands. Sandy sediments form discontinuous lenses of less than 3 m thick over the very irregular bedrock. Aeolian dunes of low elevation (< 3 m) formed on the backshore are dominated by beachgrass (*Ammophila arenaria*) and couch grass (*Agropyrum junceum*), and backed by marine pine and oak forests or by holiday cottages. Beach sediment is mostly composed of coarse to medium-sized siliciclastic particles derived from the erosion of adjacent rocky outcrops, mixed with numerous shell debris, and thinly overlays the orthogneiss substrate.

The studied area, so called Ker Chalon beach, is a 750 m long embayed coastline that features typical pocket beach characteristics: curved in plan between two headlands, low sediment supply. Ker Chalon beach, facing the mainland, is protected from the SW to NW Atlantic swell and

thus is subject to a moderate wave climate issue from the wave refraction around Yeu Island. Tides are semi diurnal and high-mesotidal to low-macrotidal with a mean range of 3.5 m (from 1.4 to 5.5 m). This hydrodynamical context allows Ker Chalon beach to display a large flat dissipative profile in the lower beach, comprised of fine sands developing under the swash at low tide, and a relatively narrow steep reflexive profile in the upper beach, with interlayers of fine sands, coarse sands and gravels (functioning under the breaking waves at high tide).

*2.2. Sampling collection*

Seawater and pore water chemistry of the Ker Chalon beach was monitored during spring tide periods between the 16$^{th}$ and the 18$^{th}$ of October 2012, and between the 8$^{th}$ and the 11$^{th}$ of April 2013. The weather was rainy during both campaigns. For both campaigns, topography of the beach was measured cross-shore using an optical level, from the foot of the dune to the water line at low tide (Fig. 1). Profile elevations are given in reference to the Chart datum (mean lower low water).

For both campaigns, we applied three different techniques to get pore water properties of three successive days. To obtain a beach water table cross-shore transect, pore waters were sampled at the top of the water-saturated zone along parallel transects during the midday low tide (Fig. 1). In addition, pore waters were collected every 10 cm depth using 1-m long home-made vertical sampling collectors deployed at four sites at increasing distances from the dune foot. Autonomous $O_2$ probes were buried in the water-saturated sand for the whole duration of the field campaigns.

Pore waters from the top of the water-saturated zone were sampled according to Anschutz et al. (2009), and Charbonnier et al. (2013). Briefly, holes were dug every 10 m along a cross-shore transect from the low-tide swash zone to the high-tide watermark. Seawater samples were collected at the beginning of each transect. The water-saturated zone of sediment was reached with one shovelful in the lower beach because sand was water-saturated up to the surface, whereas we had to dig holes more than 0.5 m deep in the upper beach to reach the saturated zone. The first water that filled the bottom of the hole was removed with a polypropylene beaker. Due to the permeability of sand, holes refilled slowly and the measurements were performed on the replenish water. Temperature, salinity, pH, and dissolved oxygen saturation were directly recorded in the waters of the excavated holes within one minute using WTW probes. The probes were calibrated before and after each field campaign using an aerated solution (100% saturation) for the oxygen saturation, an IAPSO seawater and deionized water for the salinity, and with NBS standard solutions (pH =4.01 and pH = 7.00) for the pH. Oxygen and salinity probes were compensated automatically for *in-situ* temperature. Waters were sampled using a 50-mL syringe and filtered through a 0.45 µm cellulose acetate syringe-membrane. One subsample was acidified with a 1% equivalent volume of concentrated HCl for later analyses of dissolved inorganic phosphorus (DIP), dissolved iron and

manganese; another subsample was kept frozen until later analyses of other dissolved nutrients (ammonium, nitrite, nitrate and dissolved silica (DSi)). We stored samples for the total alkalinity (TA) in polypropylene bottles after filtration using a syringe equipped with glass fiber filter (0.7 µm). The stable isotope signature of the dissolved inorganic carbon ($\delta^{13}$C-DIC) was measured in waters of the first campaign. The $\delta^{13}$C-DIC samples were collected using 120 mL glass serum bottles sealed with a rubber stopper and poisoned with 0.3 mL of $HgCl_2$ at 20 g $L^{-1}$ to avoid any microbial respiration during storage. Vials were carefully sealed taking care that no air remained in contact with samples. Vials were also stored in the dark to prevent photo-oxidation. Several samples of the solid fraction from the holes of the cross-shore transect were sampled in October 2012 in order to measure particulate organic carbon (POC) and inorganic carbon (PIC), inorganic phosphorus and reactive particulate iron and manganese concentrations.

Vertical profiles of pore water composition were obtained along a cross-shore transect at two stations in October 2012 (stations 1 and 3) and at four stations in April 2013 (Fig. 1). Each station was equipped with a pore water collector. The device was made with 1.2 m long and 10 cm diameter PVC tube pierced every 10 cm on the height. Tygon® tubes (6 mm ID) were installed inside the PVC tubes to connect each orifice to the top of the collector. The maximum dead volume was 30 mL for the longest tubes. A 100 µm mesh was put to the end of each tube in contact with sand to prevent blocking during the sampling. Pore water collectors were positioned 5 m away from the cross-shore transects described above. The upper station (station 4) was located 22 m off the dune foot in April 2013. The other stations were aligned cross-shore in the seepage face, 30 m or 20 m away one from another (Fig. 1B). Station 3 was located in an area highly colonized by sandworms (*Arenicola marina*). 20 mL pore waters were collected with syringes trough each tube after discarding the corresponding dead volume to rinse the sampling device. The sampling was always performed from the topmost surface level to deepest levels to avoid vertical mixing of pore waters. Collectors were installed the day before starting the sampling. Collection of pore waters started on the falling tide, just after the emersion of each station, and was repeated every 2-3 h until immersion of each station during flood tide. Oxygen saturation and temperature were measured immediately after pore water collection using a FireSting $O_2$ meter equipped with microOptode and temperature probe (*PyroScience GmbH*). Since these probes were available only during the second campaign (April 2013), oxygen saturation was not measured in samples of vertical pore water collector during the first campaign (Oct. 2012). The microOptode was calibrated daily for the oxygen saturation using an aerated seawater solution (100% saturation). Oxygen microOptode was compensated automatically for water temperature. Water samples were filtered through a 0.2 µm cellulose acetate syringe-membrane. One subsample was acidified with 10 µL of concentrated $HNO_3$ per 10 mL for later analyses of DIP, dissolved iron and

manganese, salinity and sulphate; another subsample was kept frozen until later analyses of dissolved inorganic nitrogen compounds (ammonium, nitrite and nitrate).

Autonomous probes equipped with a data logger were buried directly into the sediment during 2 or 3 days at each campaign according to Charbonnier et al. (2016). Four stations were examined simultaneously along the cross-shore profile (Fig. 1B). In October 2012, station 1 and 2 were located in the lower beach at 102 and 72 m from the dune foot, respectively. Station 3 located 42 m from the dune was in a beach portion highly colonized by *Arenicola marina*. Station 4 was located on the upper beach. In April 2013, the stations were located at the same distance from the dune foot than the pore water collectors. The depth at which the probes were buried was in top 20 cm of the water table at low tide, i.e., at 20±5 cm depth in the lower beach and at 60±5 cm depth in the upper beach. They measured continuously water pressure that is converted in water head (CeraDiver sensors, Schlumberger®, precision of ±0.2 cm), salinity (STPS 100SI loggers, *NKE instrumentation*; precision of ±0.1), water temperature and dissolved oxygen concentration (SDOT300 logger, *NKE instrumentation,* equipped with an Aanderaa optode model 3835; precision of ±0.05 °C and ±5 % respectively, without oxygen consumption or significant drift). Each probe recorded pore water parameters *in-situ* every 2 min. Note that optodes were placed in water during 24 h before burial to moisten their foil as recommended by Aanderaa.

*2.3. Analyses*

For pore waters sampled at the top of the water-saturated zone, the dissolved inorganic compounds were analysed colourimetrically according to standardized techniques. $NO_2^-$ and $NO_3^-$ were analysed according to Schnetger and Lehners (2014). Precision was ± 5% for $NO_2^-$ and ± 10% $NO_3^-$. DSi and DIP were measured by colorimetric procedures (Mullin and Riley, 1955; Murphy and Riley, 1962). Ammonium and DIC (only for Oct. 2012 samples) were analysed with the FIA method described by Hall and Aller (1992). The frozen subsample was defrosted on the day of the nitrite, nitrate and ammonia analyses. The subsample was allowed to stand at room temperature for at least 24 h for depolymerization of silica before carrying out DSi analysis. The obtained precision of these procedures was ± 5%. DIP was analysed on the acidified sample to prevent dissolved Fe(II) oxidative precipitation and subsequent post-sampling phosphate sequestration on Fe(III) phases. Dissolved iron ($Fe^{2+}$) was analysed by colourimetry by adding a ferrozine solution in an aliquot (Stookey, 1970). Total dissolved manganese was determined colourimetrically using the Cd-TCPP complex according to Madison et al. (2011) and Charbonnier and Anschutz (2019). Dissolved Fe and Mn were determined with ± 5% precision.

For samples collected with vertical pore water collectors, nitrate, nitrite, and ammonium were measured using standard methods on a QuAAtro AutoAnalyzer (*Seal Analytical*). DIP was measured on the acidified sample by colourimetric method of Murphy and Riley (1962). Measurements of dissolved Fe, Mn, S and Na were performed by an ICP-OES ICAP 6300 Thermo-Fischer after a 50-fold dilution with a 1% ultrapure nitric acid. Analysed elemental sulphur was interpreted as sulphate since sulphide is volatile and was removed from the sample solution under acidic conditions. Salinity was calculated from sodium concentration.

TA of surface water table samples were analysed on filtered samples by automated electro-titration on 50 mL filtered samples with 0.1N HCl as titrant. The equivalence point was determined from pH between 4 and 3 with the Gran method (Gran, 1952). Precision based on replicate analyses was better than ±5 µmol $L^{-1}$. We calculated the partial pressure of $CO_2$ ($pCO_2$) from TA, pH, and water temperature measurements using the carbonic acid dissociation constants of Millero (1979) and the $CO_2$ solubility from Weiss (1974) from the CO2SYS software (Lewis and Wallace, 1998). The $\delta^{13}$C-DIC measurements were performed with the headspace technique using a isotope ratio mass spectrometer coupled to an elemental analyser (EA-IRMS, Micromass IsoPrime) as described in Gillikin and Bouillon (2007).

The grain-size distribution was measured using a Malvern laser diffraction particle size analyser. The freeze-dried solid fraction was homogenised for chemical analyses. POC was measured by infrared spectroscopy (LECO 200 C-S analyser) after removal of carbonates with 2M HCl from 50 mg powdered sample (Etcheber et al., 1999). Total particulate carbon was measured with the same technique, on aliquots that were not acid-leached. PIC converted into $CaCO_3$ was deduced from the difference between total carbon and POC. Detection limit was 0.2‰. The precision of measurements was better than 5%. One gram crushed bulk sediment was leached with a 1N HCl solution to extract reactive P, Fe, and Mn adsorbed on particles and precipitated as oxide, carbonate, and phosphate minerals (Anschutz et al., 2005; Kostka and Luther, 1994). Extracted iron, manganese, and phosphorus contents were analysed colourimetrically according to standardized techniques with ±5% precision (Anschutz and Deborde, 2016; Charbonnier and Anschutz, 2019).

## 3. Results

### *3.1 Beach morphology and sediment characteristics*

Ker Chalon beach was 140 m wide at low tide in October 2012 and 130 m in April 2013 (Fig. 1). The difference was due to the spring tide amplitude, which was higher in October (4.8 m) than in April (4.4 m). The beach profile changed between autumn 2012 and spring 2013. In autumn, the beach showed a slightly convex to almost linear profile with a relatively steep gradient (7%) normally

resulting from summer aggradation. At 20 m from the dune foot, an erosional step of about 0.5 m high was dug at the upper limit of wave run-up at high tide. This kind of feature in the upper foreshore indicated the beginning of the winter erosion processes. The upper part of the beach was eroded in April relative to the measurements carried out 6 months earlier. In spring, the beach showed a concave profile with a slope break at 30 m from the dune foot, dividing the beach into two distinct parts. The upper foreshore was 2 m below the topographic profile measured in October with a slope of 17%, whereas the very flat lower foreshore displayed a dissipative morphodynamic beach state with a slope of 2%. A source of seeping waters appeared at the slope break at low tide. The lower beach remained always wet during tidal emersion. A continuous longshore zone of 5 to 10 m width located at the upper part of the seepage face was highly inhabited by *Arenicola marina* both in October and April (Fig.1), as evidenced by the presence of 2 to 10 fecal mounds per $m^2$. The bedrock, located at several decimetres below the topographic surface was not reached with the sampling devices.

The particle size showed a large degree of heterogeneity between the upper and the lower beach. The upper beach was composed of very permeable coarse sands and gravels, whereas the surface sediment of the seepage zone, which constituted the main part of the studied beach, consisted of well sorted particles composed of fine sand with a median grain size of 166±10 µm (Table 1) and a POC concentration of 0.20±0.08% (166±70 µmol $g^{-1}$), and a $CaCO_3$ content of 18.2±4.6% (15167±3833 µmol/g). Reactive inorganic Fe, Mn, and P concentrations were 48.6±3.5 µmol $g^{-1}$, 1.21±0.20 µmol $g^{-1}$, 12.1±2.8 µmol $g^{-1}$, respectively (Table 1). Sediment colour was light olive grey (5Y 7/2) over the first 10 cm and grey (5Y 5/1) below. Hydraulic conductivity was not measured in sands of the Ker Chalon beach but several empirical formulae allow to estimate this parameter based on grain size distribution (Vienken and Dietrich, 2011). The USBR formula (Vuković and Soro, 1992) gave 2.4 m $d^{-1}$ whereas the Seelheim (1880) formula gave 8 m $d^{-1}$. Ker Chalon beach is thus an original example of an aquifer with a high tidal range, medium energy, gentle slope and medium permeability.

*3.2. Water head measurements*

As expected, water head levels increased during flood and decreased during ebb (Fig. 2). In the seepage zone of the lower beach (stations 1 to 3), water level was almost constant at low tide during emersion of the stations (Fig. 2), because the whole sediment column remained saturated with water. For these three stations, the water head was the sediment surface. In the upper beach (station 4), the water head slowly decreased as sediment emerged.. The drop in water level occurred in the porous medium due to the exfiltration of water downslope. It decreased continuously until the

308 flooding of the next tide. The upper beach sediments were unsaturated in water down to 80 cm at
309 low tide (Fig. 2).
310
311 *3.3. Temperature and salinity*
312 Seawater and pore water temperature was relatively constant, around 16 °C in October 2012
313 and between 9 and 11 °C in April 2013. Pore water salinity remained close to 34, which was similar to
314 the value measured in seawater (Fig. 3). Some surface pore waters showed lower values around 30.
315 Vertical profiles from collectors indicated that salinity remained around 33-34 in the middle part of
316 the beach, at stations 2 and 3 (Fig. 4). Nevertheless, brackish waters were detected in April 2013 in
317 the upper beach below 1 m depth (station 4 with salinity around 30) and below 40 cm depth in the
318 lower beach (station 1 with salinity down to 23). Profiles were steady during time series of sampling
319 with pore water collectors (Fig. 4). Continuous measurements with probes located in the upper part
320 of the water-saturated zone also showed constant (±1) salinities, except at station 4 in April 2013,
321 where slightly lower salinities were recorded after emersion period (not shown on Fig. 2).
322
323 *3.4. Dissolved oxygen records*
324 Waters collected along cross-shore profiles in the superficial part of the water table showed
325 a decrease in oxygen concentration from the upper beach to the lower beach (Fig. 3). A similar trend
326 was observed for both investigated seasons. In the upper beach section near the dune foot, oxygen
327 saturation of sediment pore water varied between 80% and 100% whereas most of the values were
328 between 20% and 40% in the lower beach section (Fig. 3). These values from holes dug in the sand
329 represented pore water samples that integrated the upper decimetre of the water table. In April
330 2013, the vertical profiles determined from pore water collectors showed that oxygen concentration
331 decreased with depth and reached a value lower than 20% below 40 cm depth at stations 1 and 2
332 (Fig. 4). This clearly showed that the sediment was divided into two parts. An upper part was
333 enriched in dissolved $O_2$, and a lower part, corresponding to the grey sand, was depleted in dissolved
334 $O_2$ and almost anoxic. Time series during emersion showed that the oxic layer displayed redox
335 oscillations, with values close to 100% saturation just after emersion, and a rapid decrease at a rate
336 of about 10–15% saturation per hour (Fig. 4). Vertical profiles were more scattered at station 3
337 inhabited by the sandworms *Arenicola marina*. They also showed a decrease in $O_2$ saturation during
338 emersion, but waters remained oxic down to 1 m depth (Fig. 4). At station 4, the water table
339 deepened during emersion and pore waters remained oxic. *In-situ* probes recorded oxygen changes
340 during whole tide cycles (Fig. 2). They were placed in the transition zone between oxic and anoxic
341 sediments. Probes were mainly in the anoxic part of the sediment at station 1 and at station 2 in
342 October 2012 (Fig. 2). In April 2013 at station 2, the probe buried at 20 cm depth recorded redox

oscillations, which showed an oxygen saturation decrease after emersion reaching values below 5%, in agreement with pore water collector sample data. The probe also showed that oxygen level increased abruptly about 1 or 2 hours after the start of sediment immersion in the swash zone. The maximum value remained below 25%, and this value was reached approximately 2 to 3 hours after high tide (Fig. 2): redox oscillations followed the tidal cycle with a delay of a few hours at depth. In addition, we observed a second peak of dissolved $O_2$ that occurred at low tide slack water on the decreasing shoulder of the main peak. Such double-peaks were also observed at stations 3 and 4 (Fig. 2). At these stations, oxygen saturation also changed with tide and presented oscillation of 10% amplitude.

*3.5. Nutrients*

The cross-shore profiles of dissolved nutrients ($NO_2^-$, $NO_3^-$, $NH_4^+$, DIP, DSi) of October 2012 and April 2013 had similar shapes and showed relatively low temporal variability (Fig. 3). Pore waters at the top of the water table showed opposite cross-shore profiles for nitrate and ammonium (Fig. 3). Pore water nitrate concentrations in the upper beach and in the zone inhabited by *Arenicola marina* were higher than in seawater. Most of the values were between 20 and 40 µM (Fig. 3). $NO_3^-$ remained below 10 µM in the lower beach. Vertical pore water profiles of $NO_3^-$ showed values similar to those measured in the holes of the cross-shore profiles (Fig 3 and 4). Time series of depth profiles during emersion showed that nitrate concentration in deep pore waters did not change. However, we did observe some changes in $NO_3^-$ concentration in the top 20 cm of the sediment (Fig. 4). Immediately after the station was exposed, the surface pore waters had a nitrate concentration close to that of seawater. Afterwards, the concentrations returned to the values found deeper, so that vertical profiles became homogeneous a few hours after emersion until the next immersion (Fig. 4). Nitrite concentrations were often close to the detection limit, except at the bioturbated station 3, where concentrations up to 5 µM were measured in surface pore waters (Fig. 3 and 4). Waters of surface table along the cross-shore transects were characterized by increasing gradients of ammonium, DIP, and DSi, from the upper beach to the low tide swash zone (Fig. 3). Ammonium reached 100 µM in the lowest part of the beach, downstream from station 1 (Fig. 3). Vertical pore water profiles of $NH_4^+$ showed mean concentrations similar to those measured in holes (Fig. 3 and 4). As with nitrate, $NH_4^+$ profile time-series between emersion and flood showed changes in the surface sediment with concentrations going from the value of seawater to the value measured deeper after a few hours (Fig. 4). DIP concentrations were around 10 µM in holes of the lower part of the beach, whereas they were close to seawater concentration in upper beach pore waters (Fig. 3). Here again, depth values from vertical profiles were similar to those from the holes, with concentrations close to 2 µM at the investigated stations (Fig 3 and 4). Dissolved Si cross-shore profiles had the same shape

as DIP profiles (Fig. 3). DSi concentration was below 10 µM in seawater and in holes of the upper beach, whereas a concentration of 50 µM was reached in holes of the lower beach.

*3.6. Other redox species*

In the cross-shore profiles, concentrations of dissolved Fe and Mn higher than seawater values were found in pore waters depleted in dissolved oxygen, in the lower part of the beach (Fig. 3). Presence of dissolved Fe above 10 µM occurred more particularly in samples depleted in dissolved nitrate (Fig. 3). Hence, dissolved Fe concentration was close to seawater values in the bioturbated zone of the beach and in the upper beach, and Fe and Mn concentrations reached up to 75 µM and 8 µM, respectively, in holes of the lower beach. Vertical pore water profiles of the stations 1 and 2 showed that dissolved Mn and Fe were absent in the top 20 cm sediments, and up to 3 and 6 µM below (Fig. 4). Sulphate was measured in samples from pore water collectors. Sulphate concentrations were close to the value expected from the salinity measurement, with values between 27 and 28 mM at salinity close to 33, but some low sulphate deficit relative to salinity occurred in pore waters of stations 1, 2, and 3 in April 2013 samples (not shown).

*3.7. Carbon*

Parameters linked to carbonate chemistry were only measured in waters collected in holes of cross-shore transects because the required water volume for analyses was too high to do it on samples collected with pore water collectors. These parameters were similar for the three replicate cross-shore transects realized during each campaign (Fig. 5). They also showed comparable trends in October 2012 and in April 2013. TA of seawater was 2.3 mM (Fig. 5). Values measured in cross-shore transects were close to seawater value in the permeable upper beach. TA increased up to 4 mM in the seaward direction. The pH of seawater was close to 8.0Fig. 5. Minimum values were 0.2 pH unit below seawater value in pore waters of the lower beach, except near the low tide mark in the profile of April 11$^{th}$ 2013, in which the minimum value was 7.4 (Fig. 5). $pCO_2$ calculated from pH and TA was in equilibrium with the atmosphere in seawater samples (close to 400 ppm) (Fig. 5). Values were higher in pore waters with a $pCO_2$ value varying roughly between 800 and 2000 ppm. Interestingly the lower beach pore water of April 11$^{th}$ reached a $pCO_2$ of 5000 ppm (Fig. 5). $\delta^{13}$C-DIC was only measured in samples of October 2012 (Fig. 5). Seawater $\delta^{13}$C-DIC value was 0.15 ‰. It was lighter (more negative) in pore waters than in seawater. These pore waters with low $\delta^{13}$C-DIC values were associated with high TA, with a minimum value of -7.92 ‰ measured in the sample with the highest TA value (Fig. 5).

**4. Discussion**

*4.1. Physical context of the beach*

The Ker Chalon beach aquifer was mainly composed of saline water (Fig. 3), and did not have an underlying terrestrial groundwater body, as in most of the beaches studied. The main reason is that the Ker Chalon beach aquifer has a limited vertical extent. It is a sand lens (< 3 m thick) lying on the crustal bedrock, which prevents the intrusion of terrestrial groundwater in the tidal zone. The beach aquifer is mostly recharged by tidally driven recirculation of seawater. In addition to tidal forcing, waves increase the penetration of saline waters in the beach aquifer (Robinson et al., 2014). Some brackish waters were evidenced in the lower beach, more particularly in April 2013 (Fig. 4), suggesting that some fresh water may be occasionally carried with the recirculating salt water. The freshwater mixed with recirculating seawater could be provided by meteoric waters infiltrating the low backshore dune bordering the beach.

*4.2. Vertical and horizontal gradients of biogeochemical compounds*

There was a significant difference in temperature between October 2012 (15-16°C) and April 2013 (9-12°C). However, the profiles shown in Figures 3, 4 and 5 did not indicate sufficient differences to interpret the results in terms of seasonal changes. The shape of vertical profiles looked like well-known diagenetic profiles of marine sediments, where oxidized dissolved compounds were present in pore waters close to the sediment surface (Fig. 4). Their concentration decreased with depth, and reduced and recycled compounds accumulated at depth (Fig. 4). This was particularly true at stations 1 and 2 located in the lower part of the beach. In these stations, ammonium, dissolved Fe, and Mn concentrations increased below 20 cm depth, when dissolved $O_2$ and nitrate dropped to low values (Fig. 4). These results suggest that sediment organic matter was oxidized through reactions in which the available terminal electron acceptor that yielded the maximum energy was used, as encountered in diffusion-dominated marine sediment (Froelich et al., 1979). At stations 4 and 3, located in the upper part of the beach, sediment remained oxic, and reduced compounds such as dissolved Fe and Mn kept concentrations close to those of seawater, below 2 µM, down to a depth of 1 m (Fig. 4). Nitrate concentration in these stations was higher than the value of seawater. As the pore water salinity was similar to that of seawater, higher nitrate concentrations were most likely the result of oxic mineralization of sedimentary organic matter (Charbonnier et al., 2013).

Cross-shore transects also showed horizontal concentration gradients of redox and recycled compounds across the beach (Fig. 3). Waters of the upper beach were well oxygenated. In the lower beach, the presence of reduced compounds and high concentrations of recycled nutrients indicated that organic matter was mostly mineralized through anaerobic processes such as denitrification, reduction of Mn and Fe oxides, and sulphate reduction. N:P ratio deduced from pore water $NH_4^+$:DIP ratio varied between 10 and 15 in holes of the lower part of the beach and in the vertical profiles of

station 1, suggesting that the mineralized organic matter was of marine origin. Increase in $pCO_2$ (as well as DIP and $NH_4^+$) downslope the cross-shore transect (Fig. 5) clearly indicated that more products from organic matter mineralization accumulated in the lower part of the beach. The related increase in TA downslope suggests that the part of anaerobic processes in organic matter oxidation was higher in the lower beach, as anaerobic processes create alkalinity (Kempe, 1990; Soetaert et al., 2007; Thomas et al., 2009). Denitrification and ammonification, when ammonium is not subsequently nitrified, produce alkalinity (Abril and Frankignoulle, 2001). Both processes generate one mole of TA per mole of nitrogen involved in the reaction. Sulphate reduction was suggested by a sulphate deficit in the pore water of some samples and the grey colouration of sediments below a few cm in depth, indicative of the presence of authentic iron sulphides. This process produces two moles of TA per mole of sulphate reduced to S(-II) species, either escaping to the atmosphere when sediments are exposed at low tide (Kristensen et al., 2000), or buried as Fe-sulphide. Fe(III) and Mn(III,IV) oxide reduction is a net source of alkalinity if reduced Fe(II) and Mn(II) do not precipitate again in the sediment. Carbonate mineral dissolution is also a source of alkalinity. However, this process is not in agreement with the observed increase in $pCO_2$ and the decrease in $\delta^{13}$C-DIC (Fig. 5). DIC added in pore water shifted the isotopic signature to negative values, suggesting that this additional DIC came from a lighter source of carbon. Marine carbonates have a relatively heavy signature close to 0‰, whereas organic matter has a negative signature. In addition, a graph showing the evolution of alkalinity as a function of DIC shows a slope of 0.9 (Fig. 6A). This slope reflects the stoichiometry of the predominant reactions controlling dissolved carbonate chemistry and thus can be used to infer which reactions control dissolved carbonate chemistry (Cai et al. 2003; Liu et al. 2017). This slope would be 2 if the increase in alkalinity was due to the dissolution of carbonates. A slope close to 1 is compatible with denitrification and sulphate reduction processes. All of these results strongly suggest that the carbon added to the interstitial waters came from anaerobic mineralization of sedimentary organic matter. This result means that the studied beach is a source of alkalinity, as are larger systems such as the Wadden Sea intertidal zones (Beck et al., 2008, Santos et al. 2015). Therefore pocket beaches may account for the alkalinity budget of coastal ocean, and as a net total alkalinity generation setting, they have the potential to increase the capacity of the coastal ocean buffer and the uptake of atmospheric carbon dioxide (Hu and Cai, 2011; Brenner et al., 2016; Voynova et al., 2018).

Respiration processes in the beach aquifer occur when labile organic matter is present. A Keeling-like diagram, where $\delta^{13}$C-DIC is plotted vs. 1/DIC concentration (Pataki et al., 2003), was used to determine the isotopic composition of the organic carbon source respired in beach sediments. Concentration and $\delta^{13}$C-DIC in pore waters could be explained by a mixture of seawater DIC with a lighter source of additional DIC with a mean isotopic signature of -12.2‰±0.6‰ (Fig. 6B). This value

is less negative than marine phytoplankton isotopic signature (−22.7‰±0.8; Dubois et al., 2012) and is close to the isotopic value of marine and saltmarsh angiosperms (−11.9‰±1.4; Dubois et al., 2012), as well as macroalgae such as seaweeds (−18.8‰±2.6; Dubois et al., 2012) from neighbouring rocky shores and *Ulva sp.* (-11.1‰±1,8; Riera et al., 1996), suggesting that the carbon mineralized in pore waters came from the sea or the seashore, and not from land sources, such as terrestrial higher plants and river SPOM (−28.0‰±1.3; Dubois et al., 2012). It may have resulted from marine plant debris left on the beach at high tide (also known as wracks) mixed with the sand during seasonal erosion-accretion episodes or sand remobilization due to waves. Wracks, of which small piles have been observed on the beach, may have represented here a source of labile organic matter as observed in other beach aquifers ( Dugan et al., 2011; Lastra et al., 2018).

*4.3. Pore water residence time*

The role of water residence time on biogeochemical processes was pointed out in several studies focussing on seawater recirculation (e.g., Billerbeck et al., 2006; Waska et al., 2019). The studied transects covered oxic to anoxic redox-conditions as it has been described for other beaches (e.g. Reckhardt et al., 2015). The existence of the well-developed horizontal redox zonation from oxic to anoxic conditions towards the sea in the beach aquifer implied either that organic matter fuelling biogeochemical reactions was not the same, or that physical controls differed between the upper and the lower beach. We have measured similar concentrations of organic matter along the transect and we did not observe a gradient of $\delta^{13}$C-DIC end-member, suggesting that the origin of organic matter was not the variable that explained the horizontal redox gradient. Field observation suggests that water residence time was the main parameter that explained differences in biogeochemical processes. The water table of the upper beach dropped at each low tide (Fig. 2), indicating that the porous environment of the upper aquifer transiently filled with air was replenished with seawater at each tide. This zone was infiltrated by well-oxygenated, low-nutrient seawater at each flood. During ebb tide, a part of the pore water was flushed towards the sea, leaving the sand water unsaturated until depth around 80 cm at station 4 (Fig. 4). Deep layers of the upper beach aquifer that remained water-saturated, sampled at low tide in holes and at the bottom of pore water collectors, had a residence time sufficiently long to become enriched in dissolved nitrate, slightly enriched in DIP and DSi, but not long enough to become anoxic.

The upper beach acted as the recharge zone of the beach aquifer. Seawater infiltrated the beach face during flood faster than it discharged during ebb. Hence, the time-averaged beach water table was higher than the mean sea level (Turner et al., 1997), creating a seaward hydraulic gradient at low tide. Pore water circulated into the beach aquifer and seeped out in the lower intertidal zone (Horn, 2006; Robinson et al., 2007; Xin et al., 2015). In the Ker Chalon beach, the seepage face

518 represented almost all the beach, from 40 m off the dune foot to the low tide mark located 100 m
519 seaward farther. The fact that the water table height was almost equal to the lower beach surface is
520 characteristic of fine sand beaches (Horn, 2006). The upper part of the seepage face, at 40 m from
521 the dune foot corresponded to the portion that was highly inhabited by *Arenicola marina*. It was oxic
522 down to 1 m depth (Fig. 4), suggesting that this section of the beach received pore waters from the
523 recharge zone as a result of the seaward hydraulic gradient that occurred at low tide. In this portion
524 of the beach, oxygen concentrations showed a reverse profile after 5 hours of exposure with
525 concentrations at depth between 40 and 90 cm that were higher than those between 10 and 40 cm
526 (Fig. 4). The ventilation of the deep layer was not due to *Arenicola marina* bioirrigation because
527 worm activity does not reach the sediment deeper than 40 cm depth (Meysman et al., 2005). Deep
528 ventilated waters most likely came from the recharge zone and flowed towards the lower beach
529 aquifer during low tide.
530 Oxic waters were only present in the first decimetres of the lower beach aquifer (Fig. 4).
531 Below 30 cm depth, concentrations of reduced compounds (dissolved Fe and Mn) and metabolic
532 products (ammonium, DIP, DSi) increased seaward. This suggests that waters flowing seawards in the
533 beach aquifer became depleted in dissolved oxygen and nitrate because these waters were old.
534 Oxygen was consumed and denitrification occurred before waters were flushed through tidally-
535 driven recirculation. Considering the value of hydraulic conductivity estimated from grain size of fine
536 sand (between 2.4 and 8 m $d^{-1}$), and the slope of the beach, the Darcy velocity was between 1 and 3
537 cm $h^{-1}$. This meant that pore water covered only a few centimetres seawards during each low tide.
538 This is in agreement with the fact that profiles from pore water collectors sampled three consecutive
539 days at each campaign remained relatively constant below 30 cm depth. The estimated Darcy
540 velocity implied that anoxic pore waters found in the lower beach aquifer originated from seawater
541 that entered the upper beach sand several months before sampling. Such a low renewal of pore
542 water in the lower beach explains why waters became anoxic and enriched in metabolic products. It
543 also suggests that rain waters that infiltrated the sand in the upper beach and in the dune aquifer
544 were not totally diluted in saline pore water because of its low renewal. This may explain why we
545 found brackish pore waters at some places of the lower beach. The fresh water end-member
546 probably originates from rain events that occurred several months before seeping.
547
548 *4.4. Tidal-scale dynamics*
549 Continuous probe records of dissolved oxygen saturation and vertical profiles of some
550 chemical components revealed a tidal dynamics of pore water in the first centimetres of the lower
551 beach aquifer. Results showed that dissolved oxygen concentration increased abruptly when flood
552 tide reached the studied stations (Fig. 2). Thus, sudden ventilation of pore waters corresponded

553 probably to wave swash-induced infiltration of seawater. Several studies have determined the
554 dynamics of the swash zone moisture. Studies focusing on the estimates of swash infiltration into
555 unsaturated sand (e.g. Heiss et al., 2014; Masselink and Turner, 2012; Steenhauer et al., 2011)
556 showed that a water table mound thus formed was a consequence of a rapid rise in water content
557 during rising tide. Seawater inflow was the highest near high tide as observed at station 4 located
558 close to the high-tide water mark (Fig. 2). In most of the beach aquifer, from station 3 to the lower
559 part of the beach, the sediment remained water-saturated up to the sediment surface at low tide. In
560 this situation, the beach could behave as an impermeable surface (Packwood, 1983). Nevertheless,
561 our observations suggest that swash-induced dynamics consisted of a replacement of pore waters by
562 seawater in the upper 10–20 cm of sediment. It has been shown that waves caused cyclic infiltration-
563 exfiltration corresponding to vertical flow across the sediment surface in saturated sediments
564 (Turner and Masselink, 1998). More generally, pressure gradients due to wave generate fluxes across
565 the sediment-water interface as observed in many different contexts (Huettel et al., 2014; Riedl et
566 al., 1972; Santos et al., 2012; Shum and Sundby, 1996). Therefore, ventilation of the upper 10–20 cm
567 sediment surface was the result of pore water-seawater mixing in the swash zone during flood and
568 ebb tides, and also during the period of immersion, due to wave-induced pressure gradients (wave
569 pumping). The increase in the intensity of this pump resulted in better irrigation and ventilation of
570 the submerged sands and a deepening of the redox front (McLachlan and Turner, 1994; Riedl et al.,
571 1972). Probes deployed at stations 1 and 2 showed very low concentrations of dissolved oxygen (Fig.
572 2), probably because they were placed at a depth at the limit of the influence of wave-induced water
573 mixing. However, the periodic ventilation due to swash and immersion at each high tide could be
574 seen clearly (Fig. 2).

575 The evolution of concentration profiles during emersion was observed from the hourly
576 sampling of pore waters (Fig. 4). Pore waters collected at the beginning of beach exposure period
577 were similar to seawater in the upper 10–20 cm. In this layer, oxygen concentration decreased
578 rapidly except at the very surface of the sediment, which remained in contact with atmosphere. This
579 observation has been made for the three periods of low tide monitored the $9^{th}$, $10^{th}$ and $11^{th}$ April
580 2013, confirming that ventilation of pore waters occurred at each high tide. The rapid shift in oxygen
581 concentration at low tide corresponded to a loss of more than 100 µM in less than 5 hours at 10 cm
582 depth at stations 1, 2, and 3. This change could not alone be explained by *in-situ* aerobic respiration
583 process confined in the upper part of the aquifer, because such an efficient respiration rate would
584 also have occurred at high tide, which was not the case. Oxygen loss due to aerobic respiration would
585 have been consistent with an increase in nitrate concentration, which was also not the case at
586 stations 1 and 2 (Fig. 4). In fact, oxygen and nitrate profile monitoring showed that surface pore
587 waters evolved within a few hours from concentrations close to those of seawater just after

exposure to values close to those found at depth, suggesting that during emersion, concentration changes were mostly due to a transport process, and not to reactions. Solute transport on a distance of several centimetres in the sandy porous media may take about 1 month for transport by molecular diffusion (Huettel et al., 2014, 1996), which is much longer than observation. Therefore, the fluxes we observed were most likely explained by vertical advection of pore water. This flow can be interpreted as the vertical component of the seepage flow due to tidally-driven circulation of pore water at low tide (Chassagne et al., 2012; Robinson et al., 2007; Rocha et al., 2009; Xin et al., 2015). Dissolved Fe, Mn, ammonium, and DIP showed constant profiles during emersion at stations 1, 2, and 3 (Fig. 4). These dissolved species had a concentration close to that of seawater in the upper 20 cm, and higher concentrations below. The gradient did not move upward during emersion (within the 10-cm vertical resolution of our sampling), unlike dissolved oxygen and nitrate. This suggests that the reduced compounds did not cross the redox boundary imposed by the depth of oxygen penetration determined by the intensity of the waves and swash.

To summarize, the coupling between wave and tidally driven circulation on the wide seepage face corresponded first to a mixture with seawater of the 10–20 cm upper pore water during flood and immersion due to swash and wave pumping, and second to a 10-20 cm advective upward flux of waters at low tide due to pore water circulation in the intertidal circulation cell (Fig. 7). Seeping waters were mostly seawater that had filled the pores in the first decimetre of the beach aquifer during the previous high tide due to waves. Nutrients and reduced compounds produced during organic matter mineralization accumulated in pore water below the interface between the layer disturbed by wave mixing and the undisturbed aquifer. The flux of these components to the seawater may have occurred each time this interface was eroded, for example when wave energy increased after a period of lower energy.

## 5. Conclusions

The Ker Chalon beach is a pocket beach with fine sand that forms a small unconfined permeable aquifer. Pore water chemistry monitoring shows that biogeochemical processes are coupled to tidally-driven recirculation. Pore water composition is progressively modified along the intertidal cross-shore transect because of the production and consumption of chemical components due to marine organic matter mineralization. Aerobic processes occur in the upper part of the beach, where pore water are young. Seawards, in the seepage area, dissolved oxygen becomes depleted and anaerobic processes continue the mineralization of organic matter in older pore waters. Therefore, the porous media located a few decimetres below the beach face shifts from oxic in the upper beach to anoxic in the lower beach. In this beach, mineralization of organic matter creates a

horizontal redox stratification, not a vertical one as commonly observed in benthic environments, because of tidal pumping.

Wave-driven advection of pore water ventilates the upper part of the aquifer along the whole cross-shore transect. A vertical redox gradient occurs in the lower beach mostly because of this advection. The redox boundary that coincides with the depth of wave influence becomes shallower during emersion due to tidal pumping, inducing a flux of pore water toward the beach face. Then, the water that seeps out the aquifer at low tide is mostly composed of oxic pore water that recently entered the upper aquifer through wave pumping.

This mechanism implies that fluxes of nutrients and of reduced compounds occur mostly during immersion when redox boundary is eroded by wave-pumping after it has been shifted upwards during the previous low tide. Therefore, an increase in wave amplitude may deepens the mixed layer and may enhance the flux toward seawater of biogeochemical solutes issuing from organic matter recycling. The low hydraulic conductivity of Ker Chalon beach does not permit a rapid renewal of pore water in the aquifer. However, both tidally-driven and wave-driven recirculation of seawater allow the beach aquifer to be a bioreactor for marine organic matter mineralization that prevents accumulation of organic matter and metabolic products. The low extension of the studied aquifer, typical of pocket beaches, limits the connection with continental groundwater, unlike many other tidal environments, even if recirculating seawater comprises a high percentage of SGD (Slomp and Van Cappellen, 2004; Knee and Paytan, 2011; Anschutz et al., 2016; Tamborski et al., 2017). As such, the beach provides the coastal environment only with recycled nutrients, and not with new nutrients. This is a distinguishing feature of pocket beaches. This general characteristic of pocket beaches, however, should not blind us to the fact that the temporal and spatial properties of SGD are site-specific (e.g., Urish and McKenna, 2004; Pain et al., 2019). As a result, it is difficult to extrapolate across all pocket beaches from a single example. Other pocket beaches now deserve to be studied and compared to the example of Yeu island described here.

**Acknowledgments**

The authors gratefully acknowledge several colleagues and students who helped during the different field experiments: Cyril Ohandja Guindir, the students of the 3d year of Licence Géosciences et Environnement (promotion 2013-2014), Eric Bénéteau, Anthony Barbe, Sabrina Bichon, Ludovic Wnuczynski, Stéphane Bujan. This project was financially supported by the French National Program ESTAFET (CNRS - INSU).

**REFERENCES**

656 Abarca, E., Karam, H., Hemond, H.F., Harvey, C.F., 2013. Transient groundwater dynamics in a coastal
657 aquifer: The effects of tides, the lunar cycle, and the beach profile. Water Resources Research
658 49, 2473-2488..
659 Abril, G., Frankignoulle, M., 2001. Nitrogen–alkalinity interactions in the highly polluted Scheldt basin
660 (Belgium). Water Research 35, 844–850.
661 Anschutz, P., Deborde, J., 2016. Spectrophotometric determination of phosphate in matrices from
662 sequential leaching of sediments. Limnology and Oceanography: Methods 14, 245-256.
663 Anschutz, P., Dedieu, K., Desmazes, F., Chaillou, G., 2005. Speciation, oxidation state, and reactivity
664 of particulate manganese in marine sediments. Chemical Geology 218, 265–279.
665 Anschutz, P., Smith, T., Mouret, A., Deborde, J., Bujan, S., Poirier, D., Lecroart, P., 2009. Tidal sands as
666 biogeochemical reactors. Estuarine, Coastal and Shelf Science 84, 84–90.
667 Anschutz, P., Charbonnier, C., Mouret, A., Deborde, J., Buquet, D., Deirmendjian, L., Poirier, D.,
668 Lecroart, P., 2016. Terrestrial groundwater and nutrient discharge across tidal sands along the
669 240 km-long Aquitanian coast. Marine Chemistry 185, 38-47.
670 Ataie-ashtiani, B., Volker, R.E., Lockington, D.A., 2001. Tidal effects on groundwater dynamics in
671 unconfined aquifers. Hydrologic Processes 15, 655–669.
672 Austin, M.J., Masselink, G., 2006. Observations of morphological change and sediment transport on a
673 steep gravel beach. Marine Geology 229, 59–77.
674 Beck, M., Dellwig, O., Liebezeit, G., Schnetger, B., Brumsack, H.-J., 2008. Spatial and seasonal
675 variations of sulphate, dissolved organic carbon, and nutrients in deep pore waters of
676 intertidal flat sediments. Estuarine, Coastal and Shelf Science 79, 307–316.
677 Beck, M., Reckhardt, A., Amelsberg, J., Bartholomä, A., Brumsack, H.-J., Cypionka, H., Dittmar, T.,
678 Engelen, B., Greskowiak, J., Hillebrand, H., Holtappels, M., Neuholz, R., Köster, J., Kuypers,
679 M.M.M., Massmann, G., Meier, D., Niggemann, J., Paffrath, R., Pahnke, K., Rovo, S., Striebel,
680 M., Vandieken, V., Wehrmann, A., Zielinski, O., 2017. The drivers of biogeochemistry in beach
681 ecosystems: A cross-shore transect from the dunes to the low-water line. Marine Chemistry
682 190, 35–50.
683 Billerbeck, M., Werner, U., Polerecky, L., Walpersdorf, E., deBeer, D., Huettel, M., 2006. Surficial and
684 deep pore water circulation governs spatial and temporal scales of nutrient recycling in
685 intertidal sand flat sediment. Marine Ecology Progress Series 326, 61–76.
686 Boudafel, M.C., 2000. A mechanistic study of nonlinear solute transport in a groundwater–surface
687 water system Under steady state and transient hydraulic conditions. Water Resources
688 Research 36 (9), 2549–2565.
689 Boudreau, B.P., Huettel, M., Forster, S., Jahnke, R.A., McLachlan, A., Middelburg, J.J., Nielsen, P.,
690 Sansone, F., Taghon, G., Raaphorst, W.V., Webster, I., Weslawski, J.M., Wiberg, P., Sundby, B.,
691 2001. Permeable marine sediments: Overturning an old paradigm. Eos, Transactions American
692 Geophysical Union 82, 133–136.
693 Bratton, J.F., 2010. The Three Scales of Submarine Groundwater Flow and Discharge across Passive
694 Continental Margins. The Journal of Geology 118, 565–575.
695 Brenner, H., U. Braeckman, M. Le Guitton, and F. J. R. Meysman. 2016. The impact of sedimentary
696 alkalinity release on the water column CO2 system in the North Sea. Biogeosciences 13: 841–
697 863.
698 Brovelli, A., Mao, X., Barry, D.A., 2007. Numerical modeling of tidal influence on density-dependent
699 contaminant transport. Water Resources Research 43, W10426.
700 Buquet, D., Sirieix, C., Anschutz, P., Malaurent, P., Charbonnier, C., Naessens, F., Bujan, S., Lecroart,
701 P., 2016. Shape of the shallow aquifer at the fresh water–sea water interface on a high-energy
702 sandy beach. Estuarine, Coastal and Shelf Science. 179, 79–89.
703 Burnett, W.C., Bokuniewicz, H., Huettel, M., Moore, W.S., Taniguchi, M., 2003. Groundwater and
704 Pore Water Inputs to the Coastal Zone. Biogeochemistry 66, 3–33.
705 Cai, W. J., Y. Wang, J. Krest, and W. S. Moore. 2003. The geochemistry of dissolved inorganic carbon
706 in a surficial groundwater aquifer in north inlet, South Carolina, and the carbon fluxes to the
707 coastal ocean. Geochimica et Cosmochimica Acta 67, 631–637.

Castelle, B., Marieu, V., Bujan, S., Ferreira, S., Parisot, J.-P., Capo, S., Sénéchal, N., Chouzenoux, T., 2014. Equilibrium shoreline modelling of a high-energy meso-macrotidal multiple-barred beach. Marine Geology 347, 85–94.

Charbonnier, C., Anschutz, P., 2019. Spectrophotometric determination of manganese in acidified matrices from (pore)waters and from sequential leaching of sediments. Talanta 195, 778–784.

Charbonnier, C., Anschutz, P., Deflandre, B., Bujan, S., Lecroart, P., 2016. Measuring pore water oxygen of a high-energy beach using buried probes. Estuarine, Coastal and Shelf Science, 179, 66–78.

Charbonnier, C., Anschutz, P., Poirier, D., Bujan, S., Lecroart, P., 2013. Aerobic respiration in a high-energy sandy beach. Marine Chemistry 155, 10–21.

Charette, M.A., Sholkovitz, E.R., 2002. Oxidative precipitation of groundwater-derived ferrous iron in the subterranean estuary of a coastal bay. Geophysical Research Letters 29, 85-1-85–4.

Chassagne, R.L., Lecroart, P., Beaugendre, H., Capo, S., Parisot, J.-P., Anschutz, P., 2012. Silicic acid flux to the ocean from tidal permeable sediments: A modeling study. Computers & Geosciences 43, 52–62.

Couturier, M., Tommi-Morin, G., Sirois, M., Rao, A., Nozais, C., Chaillou, G., 2017. Nitrogen transformations along a shallow subterranean estuary. Biogeosciences 14, 3321–3336.

Dubois, S., Savoye, N., Grémare, A., Plus, M., Charlier, K., Beltoise, A., Blanchet, H., 2012. Origin and composition of sediment organic matter in a coastal semi-enclosed ecosystem: An elemental and isotopic study at the ecosystem space scale. Journal of Marine Systems 94, 64–73.

Dugan, J.E., Hubbard, D.M., Page, H.M., Schimel, J.P., 2011. Marine macrophyte wrack inputs and dissolved nutrients in beach sands. Estuaries and Coasts 34, 839–850.

Durand, A., Fattal, P., Baltzer, A., Robin, M., Rollo, N., Le Mauff, B., Maanan, M., 2014. Campagne de mesures en mer 2013 : bathymétrie, sismique, sédimentologie et courantologie. Rapport Observatoire du Littoral des Pays de Monts, 199pp.

Etcheber, H., Relexans, J.-C., Beliard, M., Weber, O., Buscail, R., Heussner, S., 1999. Distribution and quality of sedimentary organic matter on the Aquitanian margin (Bay of Biscay). Deep Sea Research Part II: Topical Studies in Oceanography 46, 2249–2288.

Froelich, P.N., Klinkhammer, G.P., Bender, M.L., Luedtke, N.A., Heath, G.R., Cullen, D., Dauphin, P., Hammond, D., Hartman, B., Maynard, V., 1979. Early oxidation of organic matter in pelagic sediments of the eastern equatorial Atlantic: suboxic diagenesis. Geochimica et Cosmochimica Acta 43, 1075–1090.

Gillikin, D.P., Bouillon, S., 2007. Determination of δ18O of water and δ13C of dissolved inorganic carbon using a simple modification of an elemental analyser-isotope ratio mass spectrometer: an evaluation. Rapid Communications in Mass Spectrometry 21, 1475–1478.

Gonneea, M.E., Charette, M.A., 2014. Hydrologic Controls on Nutrient Cycling in an Unconfined Coastal Aquifer. Environmental Science and Technology 48, 14178–14185.

Gran, G., 1952. Determination of the equivalence point in potentiometric titrations. Part II. Analyst 77, 661–671.

Hall, P.O.J., Aller, R.C., 1992. Rapid, small-volume, flow injection analysis for SCO2, and NH4+ in marine and freshwaters. Limnology and Oceanography 37, 1113–1119.

Hays, R.L., Ullman, W.J., 2007. Direct determination of total and fresh groundwater discharge and nutrient loads from a sandy beachface at low tide (Cape Henlopen, Delaware). Limnology and Oceanography 52, 240–247.

Heiss, J.W., Michael, H.A., 2014. Saltwater-freshwater mixing dynamics in a sandy beach aquifer over tidal, spring-neap, and seasonal cycles. Water Resources Research 50, 6747–6766.

Heiss, J.W., Ullman, W.J., Michael, H.A., 2014. Swash zone moisture dynamics and unsaturated infiltration in two sandy beach aquifers. Estuarine, Coastal and Shelf Science 143, 20–31.

Horn, D.P., 2006. Measurements and modelling of beach groundwater flow in the swash-zone: a review. Continental Shelf Research 26, 622–652.

Hu, X., and W.-J. Cai. 2011. An assessment of ocean margin anaerobic processes on oceanic alkalinity budget. Global Biogeochemical Cycles 25: 1–11. doi:10.1029/2010gb003859

760 Huettel, M., Berg, P., Kostka, J.E., 2014. Benthic Exchange and Biogeochemical Cycling in Permeable
761 Sediments. Annual Review of Marine Science 6, 23–51.
762 Kempe, S., 1990. Alkalinity: The link between anaerobic basins and shallow water carbonates?
763 Naturwissenschaften 77, 426–427.
764 Knee, K.L., Paytan, A., 2011. Submarine groundwater discharge: a source of nutrients, metals, and
765 pollutants to the coastal ocean. In: Wolanski, E., McLusky, D.S. (eds.) Treatise on Estuarine and
766 Coastal Science, Vol 4, pp. 205–233.
767 Kostka, J.E., Luther, G.W., 1994. Partitioning and speciation of solid phase iron in saltmarsh
768 sediments. Geochimica et Cosmochimica Acta 58, 1701–1710.
769 Kristensen, E., Bodenbender, J., Jensen, M.H., Rennenberg, H., Jensen, K.M., 2000. Sulfur cycling of
770 intertidal Wadden Sea sediments (Konigshafen, Island of Sylt, Germany): sulfate reduction and
771 sulfur gas emission. Journal of Sea Research 43, 93-104.
772 Kroeger, K.D., Charette, M.A., 2008. Nitrogen biogeochemistry of submarine groundwater discharge.
773 Limnology and Oceanography 53 (3), 1025–1039.
774 Lastra, M., López, J., Rodil, I.F., 2018. Warming intensify CO2 flux and nutrient release from algal
775 wrack subsidies on sandy beaches. Global Change Biology 24, 3766–3779.
776 Lewis, E., Wallace, D., 1998. Program developed for CO2 system calculations. Carbon dioxide
777 information analysis center, Oak Ridge National Laboratory, Tennessee.
778 Li, L., Barry, D.A., Stagnitti, F., Parlange, J.-Y., 1999. Submarine groundwater discharge and associated
779 chemical input to a coastal sea. Water Resources Research 35, 3253–3259.
780 Li, X., Hu, B.X., Burnett, W.C., Santos, I.R., Chanton, J.P., 2009. Submarine Ground Water Discharge
781 Driven by Tidal Pumping in a Heterogeneous Aquifer. Groundwater 47, 558–568.
782 Liu, Q., M. A. Charette, C. F. Breier, P. B. Henderson, C. Mccorkle, W. Martin, and M. Dai. 2017.
783 Carbonate system biogeochemistry in a subterranean estuary-Waquoit Bay, USA. Geochim.
784 Cosmochim. Acta. 203: 422–439. doi: 10.1016/j.gca.2017.01.041
785 Liu, Y., Liang, W., and Jiao, J.J., 2018. Seasonality of nutrient flux and biogeochemistry in an intertidal
786 aquifer. Journal of Geophysical Research: Oceans, 123, 6116–6135
787 Luijendijk, A., Hagenaars, G., Ranasinghe, R., Baart, F., Donchyts, G., Aarninkhof, S., 2018. The State
788 of the World's Beaches. Scientific Reports 8, 6641.
789 Madison, A.S., Tebo, B.M., Luther, G.W., 2011. Simultaneous determination of soluble
790 manganese(III), manganese(II) and total manganese in natural (pore)waters. Talanta 84, 374–
791 381.
792 Masselink, G., Turner, I.L., 2012. Large-scale laboratory investigation into the effect of varying back-
793 barrier lagoon water levels on gravel beach morphology and swash zone sediment transport.
794 Coastal Engineering, 63, 23–38.
795 McLachlan, A., Turner, I., 1994. The interstitial environment of sandy beaches. Marine Ecology 15,
796 177–212.
797 Meysman, F., Galaktionov, O., Middelburg, J., 2005. Irrigation patterns in permeable sediments
798 induced by burrow ventilation: a case study of Arenicola marina. Mar. Ecol. Prog. Ser. 303,
799 195–212.
800 Millero, F.J., 1979. The thermodynamics of the carbonate system in seawater. Geochimica et
801 Cosmochimica Acta 43, 1651–1661.
802 Moore, W.S., 1999. The subterranean estuary: a reaction zone of ground water and sea water.
803 Marine Chemistry 65, 111–125.
804 Moore, W.S., Wilson, A.M., 2005. Advective flow through the upper continental shelf driven by
805 storms, buoyancy, and submarine groundwater discharge. Earth and Planetary Science Letters
806 235, 564–576.
807 Mullin, J.B., Riley, J.P., 1955. The colorimetric determination of silicate with special reference to sea
808 and natural waters. Analytica Chimica Acta 12, 162–176.
809 Murphy, J., Riley, J.P., 1962. A modified single solution method for the determination of phosphate in
810 natural waters. Analytica Chimica Acta 27, 31–36.

Packwood, A.R., 1983. The influence of beach porosity on wave uprush and backwash. Coastal Engineering 7, 29–40.
Paerl, H.W., 1997. Coastal eutrophication and harmful algal blooms: Importance of atmospheric deposition and groundwater as “new” nitrogen and other nutrient sources. Limnology and Oceanography 42: 1154–1165.
Pain, A.J., Martin, J.B., Young, C.R., 2019. Sources and sinks of CO2 and CH4 in siliciclastic subterranean estuaries. Limnol. Oceanogr. 64, 2019, 1500–1514
Pataki, D.E., Bowling, D.R., Ehleringer, J.R., 2003. Seasonal cycle of carbon dioxide and its isotopic composition in an urban atmosphere: Anthropogenic and biogenic effects. Journal of Geophysical Research 108, 4735.
Reckhardt, A., Beck, M., Seidel, M., Riedel, T., Wehrmann, A., Bartholomä, A., Schnetger, B., Dittmar, T., Brumsack, H.-J., 2015. Carbon, nutrient and trace metal cycling in sandy sediments: A comparison of high-energy beaches and backbarrier tidal flats. Estuarine, Coastal and Shelf Science 159, 1–14.
Riedl, R.J., Huang, N., Machan, R., 1972. The subtidal pump: a mechanism of interstitial water exchange by wave action. Marine Biology 13, 210–221.
Riera, P., Richard, P., Grémare, A., Blanchard, G., 1996. Food source of intertidal nematodes in the Bay of Marennes-Oléron (France), as determined by dual stable isotope analysis. Mar. Ecol. Prog. Ser. 142, 303–309.
Robinson, C., Baldock, T., Horn, D., Gibbes, B., Hughes, M.G., Nielsen, P., Li, L., 2006. Measurement of groundwater and swash interactions on a sandy beach. Coastal Dynamics 2005, Proceedings 1–12. https://doi.org/10.1061/40855(214)104
Robinson, C., Li, L., Prommer, H., 2007. Tide-induced recirculation across the aquifer-ocean interface. Water Resources Research 43, W07428.
Robinson, C.E., Xin, P., Li,L., Barry, D.A., 2014. Groundwater flow and salt transport in a subterranean estuary driven by intensified wave conditions. Water Resources Research 50, 1-17.
Rocha, C., Ibanhez, J., Leote, C., 2009. Benthic nitrate biogeochemistry affected by tidal modulation of Submarine Groundwater Discharge (SGD) through a sandy beach face, Ria Formosa, Southwestern Iberia. Marine Chemistry 115, 43–58.
Santoro, A.E., 2010. Microbial nitrogen cycling at the saltwater–freshwater interface. Hydrogeological Journal 18, 187–202.
Santos, I.R., Burnett, W.C., Dittmar, T., Suryaputra, I.G.N.A., Chanton, J., 2009. Tidal pumping drives nutrient and dissolved organic matter dynamics in a Gulf of Mexico subterranean estuary. Geochimica et Cosmochimica Acta 73, 1325–1339.
Santos, I.R., Eyre, B.D., Huettel, M., 2012. The driving forces of porewater and groundwater flow in permeable coastal sediments: a review. Estuar. Coast. Shelf Sci. 98, 1–15.
Santos, I.R., Beck, M., Brumsack, H.–J., Maher, D.T., Dittmar, T., Waska, H., Schnetger, B., 2015. Porewater exchange as a driver of carbon dynamics across a terrestrial-marine transect: Insights from coupled 222Rn and pCO2 observations in the German Wadden Sea. Marine Chemistry 171, 10–20.
Sawyer, A.H., David, C.H., Famiglietti, J.S., 2016. Continental patterns of submarine groundwater discharge reveal coastal vulnerabilities. Science 353, 705–707.
Schnetger, B., Lehners, C., 2014. Determination of nitrate plus nitrite in small volume marine water samples using vanadium(III)chloride as a reduction agent. Marine Chemistry 160, 91–98.
Seelheim, F., 1880. Methoden zur bestimmung der durschlassigkeit des bodens. Z. analy.chem. 387–402.
Short, A., Masselink, G., 1999. Embayed and structurally controlled beaches, in Handbook of Beach and Shoreface Morphodynamics, edited by A. D. Short, pp. 230–249, John Wiley, New York.
Shum, K.T., Sundby, B., 1996. Organic matter processing in continental shelf sediments—the subtidal pump revisited. Marine Chemistry, 53, 81–87.
Slomp, C.P., Van Cappellen, P., 2004. Nutrient inputs to the coastal ocean through submarine groundwater discharge: controls and potential impact. Journal of Hydrology 295, 64–86.

Soetaert, K., Hofmann, A.F., Middelburg, J.J., Meysman, F.J.R., Greenwood, J., 2007. The effect of biogeochemical processes on pH. Marine Chemistry 105, 30–51

Spiteri, C., Slomp, C.P., Charette, M.A., Tuncay, K., Meile, C., 2008. Flow and nutrient dynamics in a subterranean estuary (Waquoit Bay, MA, USA): field data and reactive transport modeling. Geochimica et Cosmochimica Acta 72, 3398-3412

Steenhauer, K., Pokrajac, D., O'Donoghue, T., Kikkert, G.A., 2011. Subsurface processes generated by bore-driven swash on coarse-grained beaches. Journal of Geophysical Research: Oceans. 116

Stookey, L.L., 1970. Ferrozine---a new spectrophotometric reagent for iron. Anal. Chem. 42, 779–781.

Tamborski, J.J., Cochran, J.K., Bokuniewicz, H.J., 2017. Submarine groundwater discharge driven nitrogen fluxes to Long Island Sound, NY: Terrestrial vs. marine sources. Geochimica et Cosmochimica Acta 218, 40–57.

Thomas, H., Schiettecatte, L.-S., Suykens, K., Koné, Y.J.M., Shadwick, E.H., Prowe, A.E.F., Bozec, Y., Baar, H.J.W. de, Borges, A.V., 2009. Enhanced ocean carbon storage from anaerobic alkalinity generation in coastal sediments. Biogeosciences 6, 267–274.

Turner, I.L., Coates, B.P., Acworth, R.I., 1997. Tides, Waves and the Super-elevation of Groundwater at the Coast. Journal of Coastal Research 13 (1), 46–60.

Turner, I.L., Masselink, G., 1998. Swash infiltration-exfiltration and sediment transport. Journal of Geophysical Research: Oceans 103, 30813–30824.

Ullman, W.J., Chang, B., Miller, D.C., Madsen, J.A., 2003. Groundwater mixing, nutrient diagenesis, and discharges across a sandy beachface, Cape Henlopen, Delaware (USA). Estuarine, Coastal and Shelf Science 57, 539–552.

Urish, D.W., McKenna, T.E., 2004. Tidal effects on ground water discharge through a sandy marine beach. Groundwater 42 (7), 971–982.

Vandenbohede, A., Lebbe, L., 2006. Occurrence of salt water above fresh water in dynamic equilibrium in a coastal groundwater flow system near De Panne, Belgium. Hydrogeol J 14, 462–472.

Vienken, T., Dietrich, P., 2011. Field evaluation of methods for determining hydraulic conductivity from grain size data. Journal of Hydrology 400, 58–71.

Voynova, Y.G., Petersen, W., Gehrung, M., Aßmann, S. and King, A.L. (2019), Intertidal regions changing coastal alkalinity: The Wadden Sea-North Sea tidally coupled bioreactor. Limnology and Oceanography 64, 1135-1149.

Vuković, M., Soro, A., 1992. Determination of hydraulic conductivity of porous media from grain-size composition. Water Resources Publications, Littleton, Colo.

Waska H, Greskowiak J, Ahrens J, Beck M, Ahmerkamp S, Böning P, Brumsack HJ, Degenhardt J, Ehlert C, Engelen B, Grünenbaum N, Holtappels M, Pahnke K, Marchant HK, Massmann G, Meier D, Schnetger B, Schwalfenberg K, Simon H, Vandieken V, Zielinski O and Dittmar T (2019) Spatial and Temporal Patterns of Pore Water Chemistry in the Inter-Tidal Zone of a High Energy Beach. Frontier in Marine Science 6:154. doi: 10.3389/fmars.2019.00154

Weiss, R., 1974. Carbon dioxide in water and seawater: the solubility of a non-ideal gas. Marine chemistry 2, 203–215.

Xin, P., Wang, S.S.J., Lu, C., Robinson, C., Li, L., 2015. Nonlinear interactions of waves and tides in a subterranean estuary. Geophysical Research Letters 42, 2277–2284

**Figure captions**

Figure 1: Map of the Yeu Island and location of the Ker Chalon beach (A). Graphical representation of the sampling site on the tidal beach (B). Cross-shore topographic profiles obtained in October 2012 and April 2013 with the position of pore water collectors (C)

Figure 2: Dissolved oxygen saturation and water head recorded in October 2012 and April 2013 in sediment of the Ker Chalon beach at the station along the cross-shore transect (Fig. 1). Data were obtained from autonomous probes buried in the upper part of the water-saturated aquifer at low tide.

Figure 3: Salinity and concentrations of dissolved $O_2$, nitrate, nitrite, ammonium, dissolved manganese, dissolved iron, inorganic phosphorus (DIP), and dissolved silica (DSi) in pore waters from cross-shore transects of the Ker Chalon beach in October 2012 (left column) and April 2013 (right column). Transects were replicated three times at low tide during each campaign. The position 0 m corresponds to the base of the dune. Seawater values are represented by a star at the 150 m position.

Figure 4: Vertical profiles of salinity and concentrations of dissolved $O_2$, nitrate, nitrite, ammonium, dissolved manganese, dissolved iron, and inorganic phosphorus (DIP) in pore waters from pore water collectors deployed on the Ker Chalon beach in October 2012 (left) and April 2013 (right). Sampling was replicated several times during one emersion period to monitor the evolution of measured parameters in an hourly time scale. Such sampling was repeated at two or three low tides during each campaign; the evolution was the same each time. Profiles presented here are those from samples collected in October 17$^{th}$ 2012, and April 11$^{th}$ 2013. The positions of pore water collectors indicated on Fig. 1 are represented by vertical bars.

Figure 5: Total alkalinity, pH, and $pCO_2$ values in pore waters from cross-shore transects of the Ker Chalon beach in October 2012 (left) and April 2013 (right), and $\delta^{13}$-DIC in pore waters from October 2012. Transects were replicated three times at low tide during each campaign. The position 0 m corresponds to the base of the dune. Seawater values are represented by a star at the 150 m position.

Figure 6. (A) TA concentrations versus DIC, and (B) Keeling plot of Ker Chalon beach pore waters collected in October 2012. The intercept at the origin of the Keeling plot gives the isotopic signature of the source of the mineralized organic carbon that produces additional DIC relative to seawater DIC concentration.

Figure 7: Schematic representation of hydrologic circulation during flow (left) and low tide (right) showing potential source contributing to ventilation of pore waters. 1: Parcels of meteoritic waters mixed with saline water; 2: Seeping of pore water at the slope break; 3: Vertical component of tidally-driven circulation pushing the redox gradient upwards. The dotted line indicates the boundary between the aquifer dominated by aerobic and anaerobic organic matter (OM) mineralization processes..

**FIGURE 1**

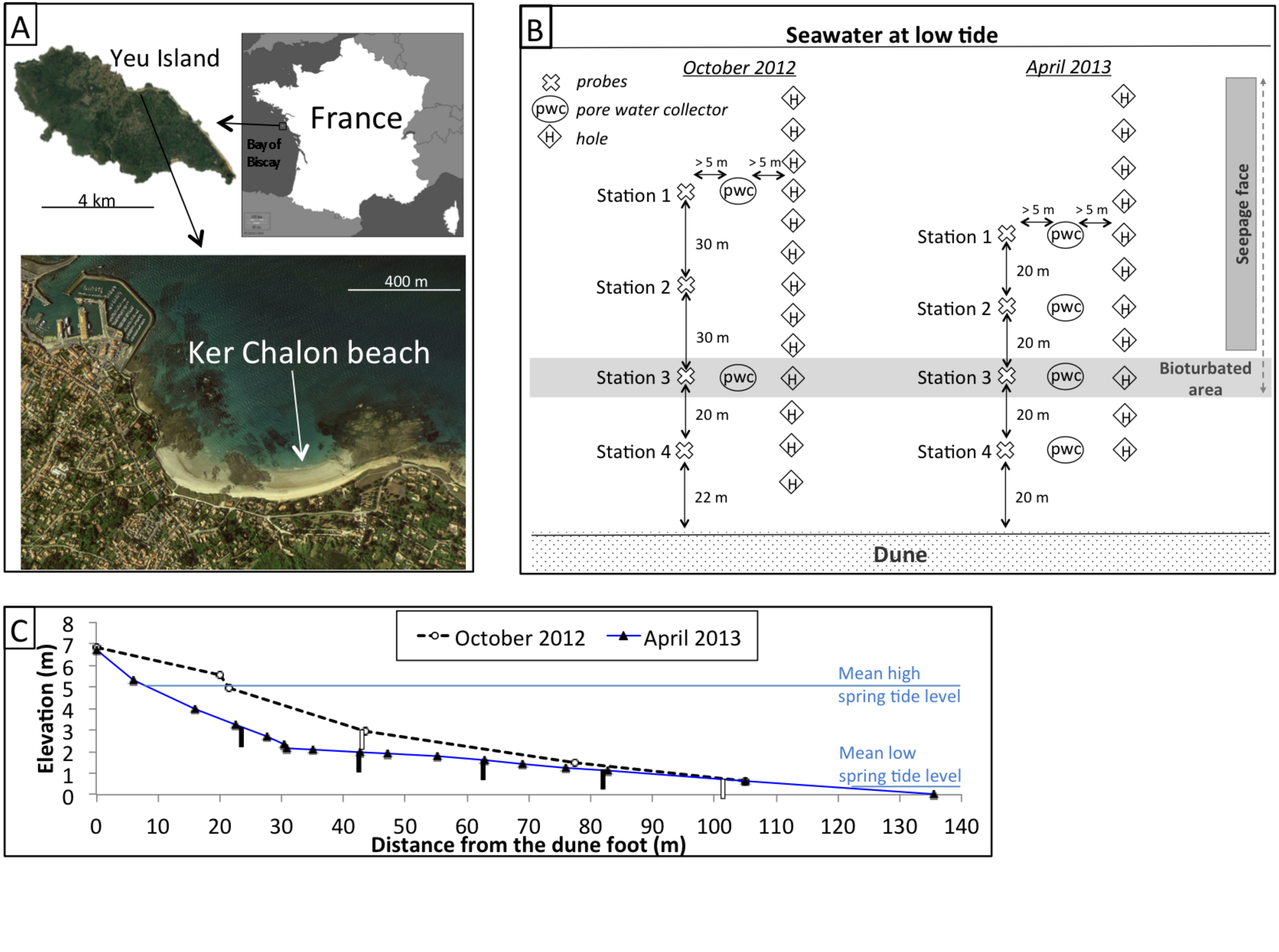
A
Yeu Island
France
Bay of Biscay
4 km
400 m
Ker Chalon beach
B
Seawater at low tide
October 2012
April 2013
probes
pore water collector
hole
pwc
H
> 5 m
> 5 m
Station 1
Station 2
Station 3
Station 4
30 m
30 m
20 m
22 m
20 m
20 m
20 m
Seepage face
Bioturbated area
Dune
C
October 2012
April 2013
Elevation (m)
Mean high spring tide level
Mean low spring tide level
Distance from the dune foot (m)

**FIGURE 2**

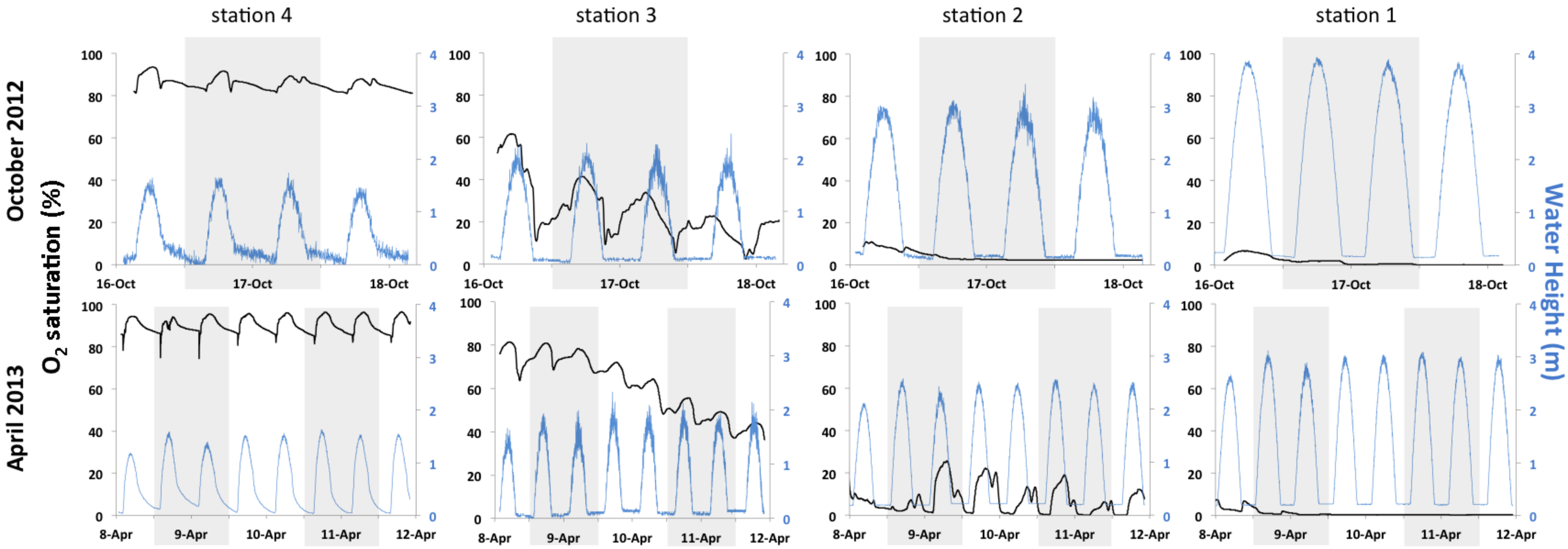
station 4
station 3
station 2
station 1
October 2012
April 2013
$O_2$ saturation (%)
Water Height (m)
16-Oct
17-Oct
18-Oct
8-Apr
9-Apr
10-Apr
11-Apr
12-Apr
0
20
40
60
80
100
0
1
2
3
4

**FIGURE 3**

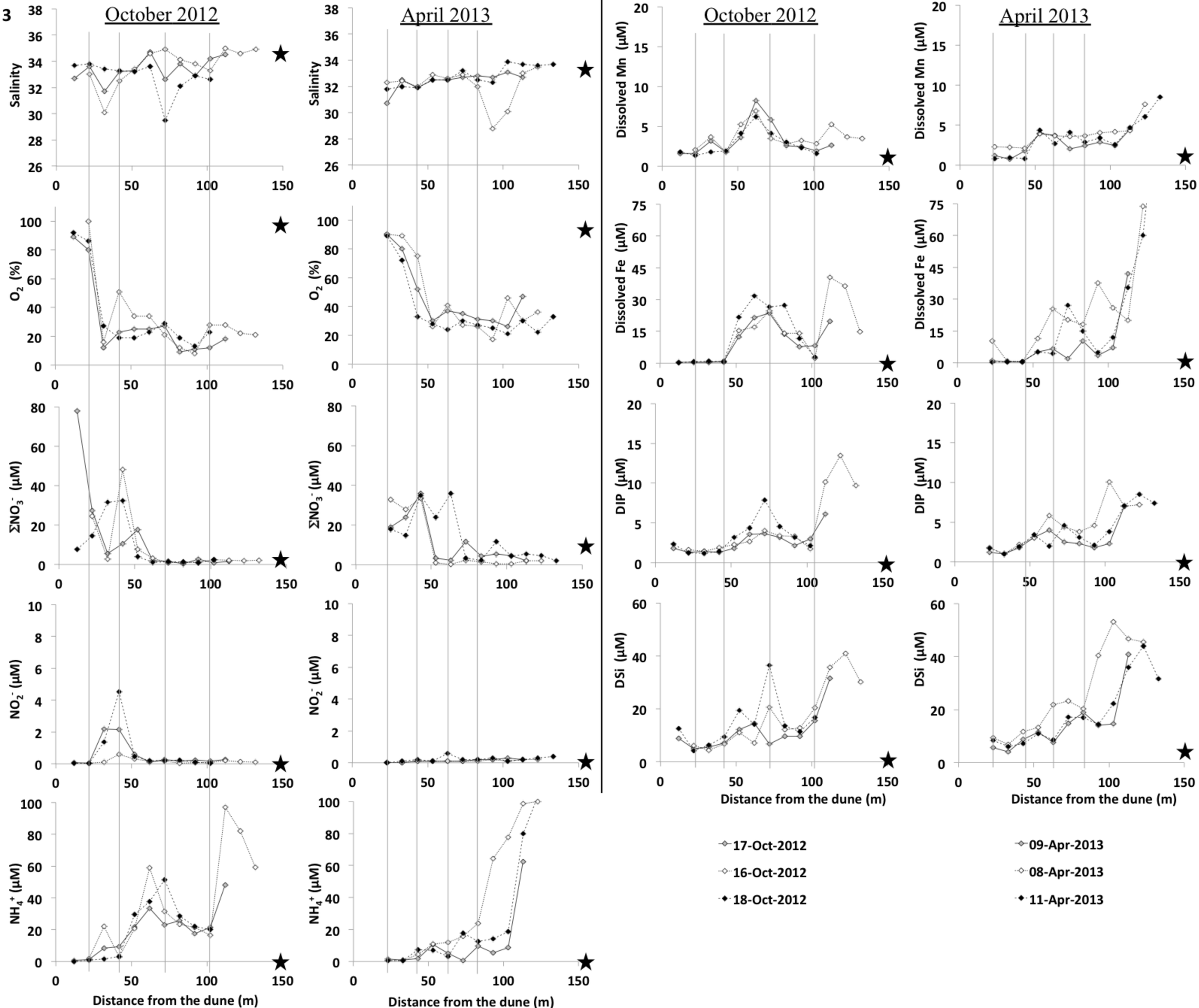
October 2012
April 2013
Salinity
Dissolved Mn (µM)
$O_2$ (%)
Dissolved Fe (µM)
DIsolved Fe (µM)
$\Sigma NO_3^-$ (µM)
DIP (µM)
$NO_2^-$ (µM)
DSi (µM)
$NH_4^+$ (µM)
Distance from the dune (m)
17-Oct-2012
16-Oct-2012
18-Oct-2012
09-Apr-2013
08-Apr-2013
11-Apr-2013

**FIGURE 4 suite**

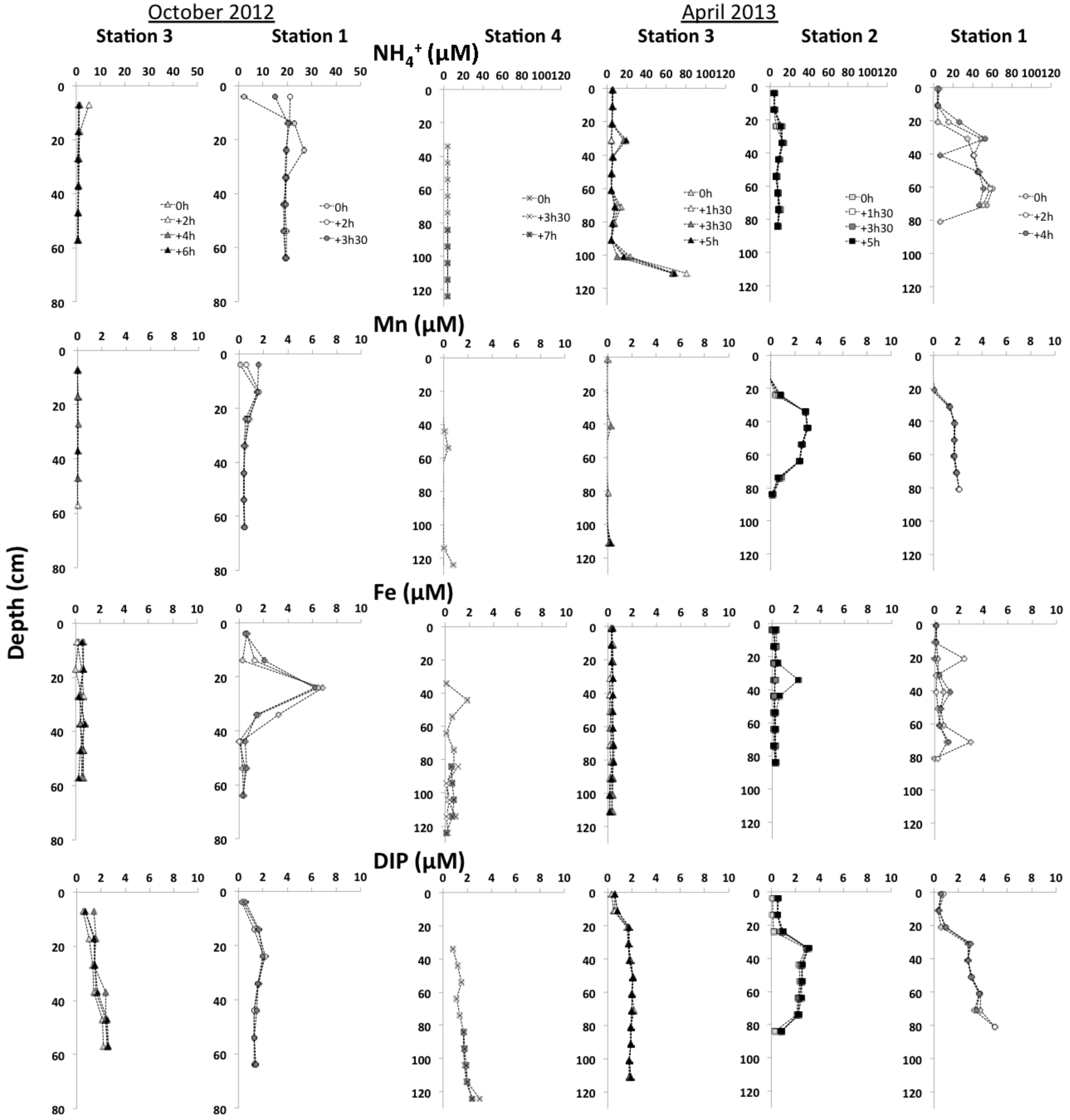

**FIGURE 4**

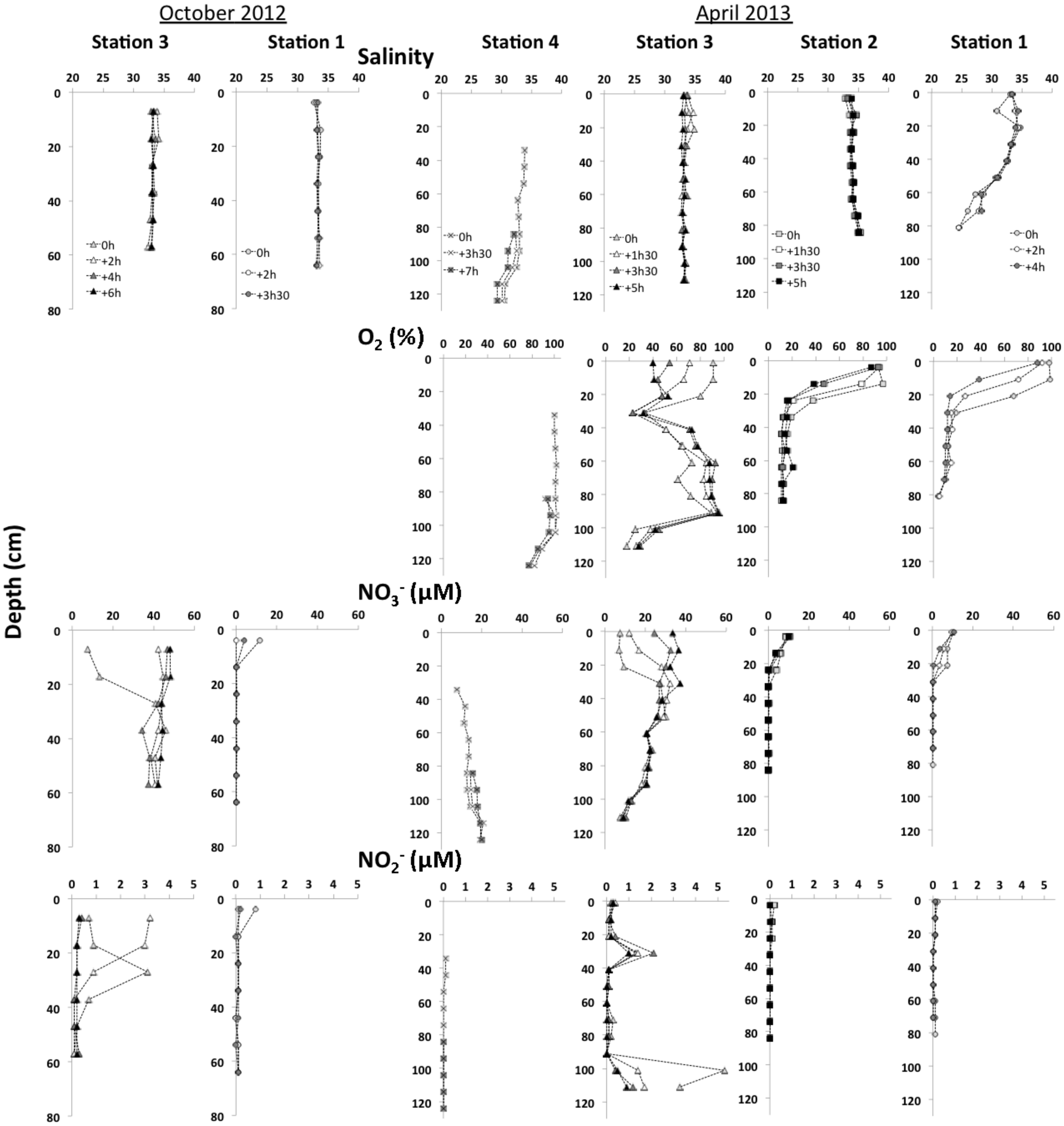
October 2012
April 2013
Station 3
Station 1
Station 4
Station 3
Station 2
Station 1
Salinity
$O_2$ (%)
$NO_3^-$ (µM)
$NO_2^-$ (µM)
Depth (cm)
0h
+2h
+4h
+6h
+3h30
+7h
+1h30
+5h

**FIGURE 5**

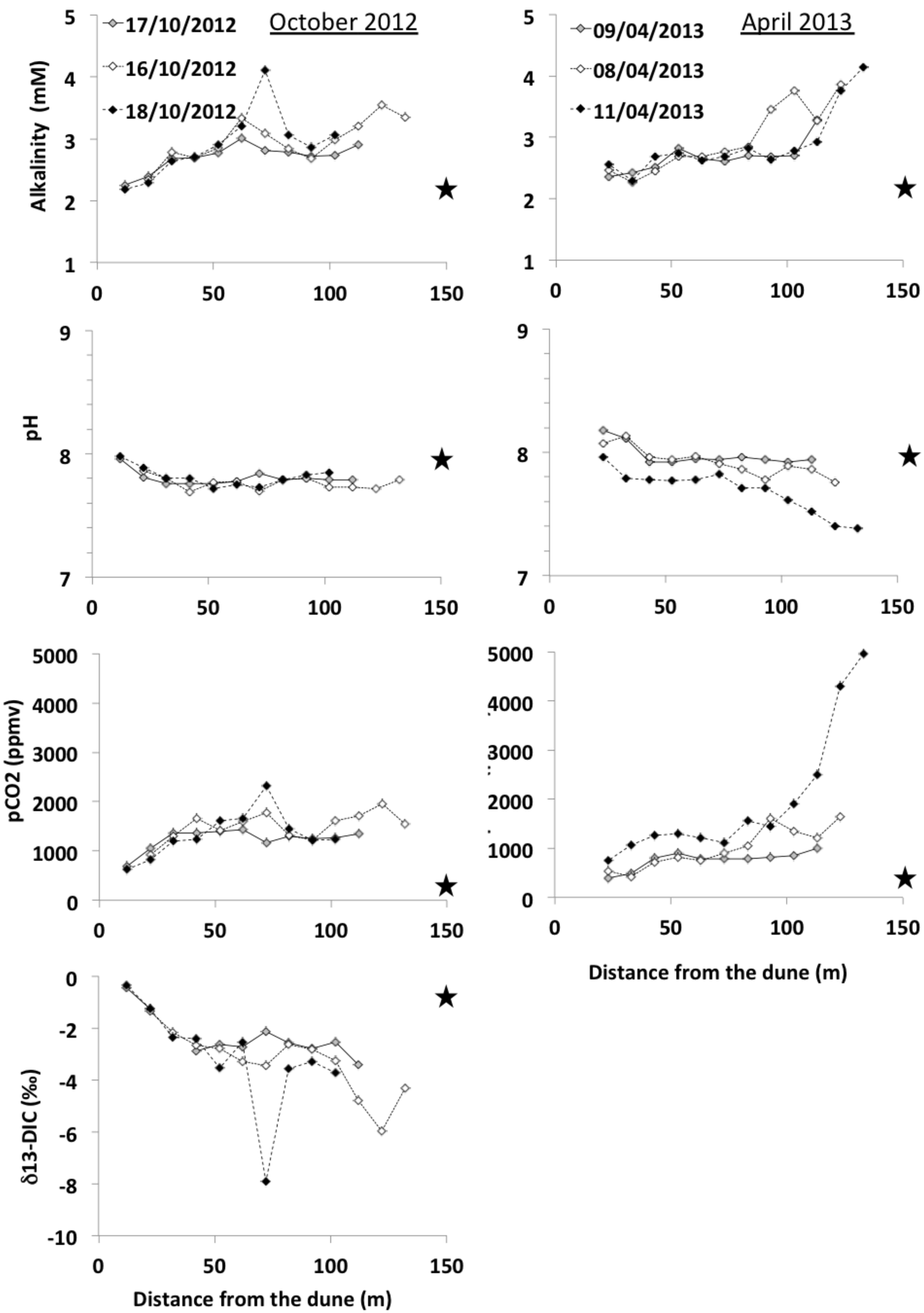
October 2012
April 2013
17/10/2012
16/10/2012
18/10/2012
09/04/2013
08/04/2013
11/04/2013
Alkalinity (mM)
pH
pCO2 (ppmv)
δ13-DIC (‰)
Distance from the dune (m)
Distance from the dune (m)

FIGURE 6

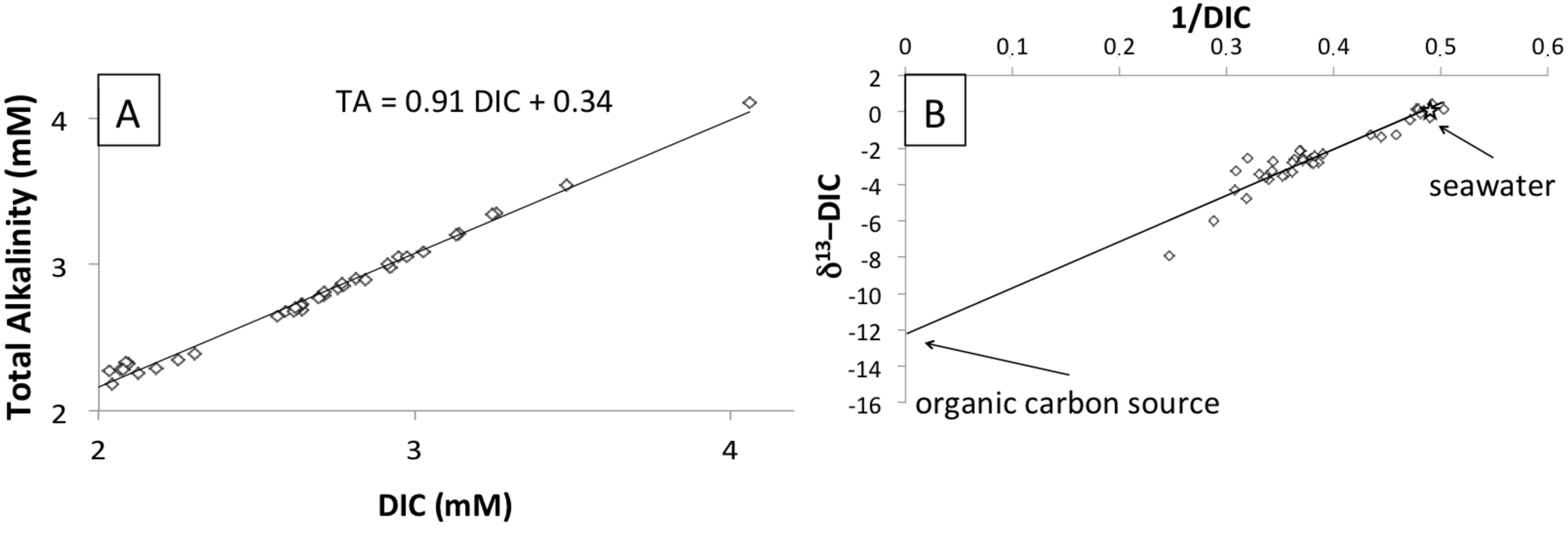
A
TA = 0.91 DIC + 0.34
Total Alkalinity (mM)
DIC (mM)
2
3
4
B
1/DIC
0
0.1
0.2
0.3
0.4
0.5
0.6
δ13–DIC
seawater
organic carbon source

**FIGURE 7**

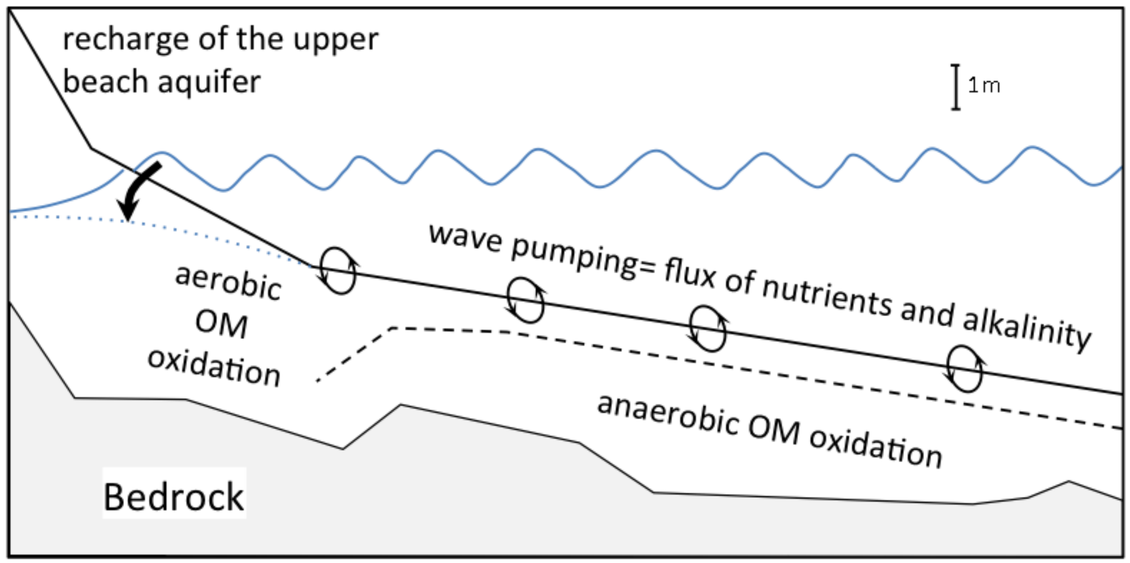
recharge of the upper
beach aquifer
1m
wave pumping= flux of nutrients and alkalinity
aerobic
OM
oxidation
anaerobic OM oxidation
Bedrock

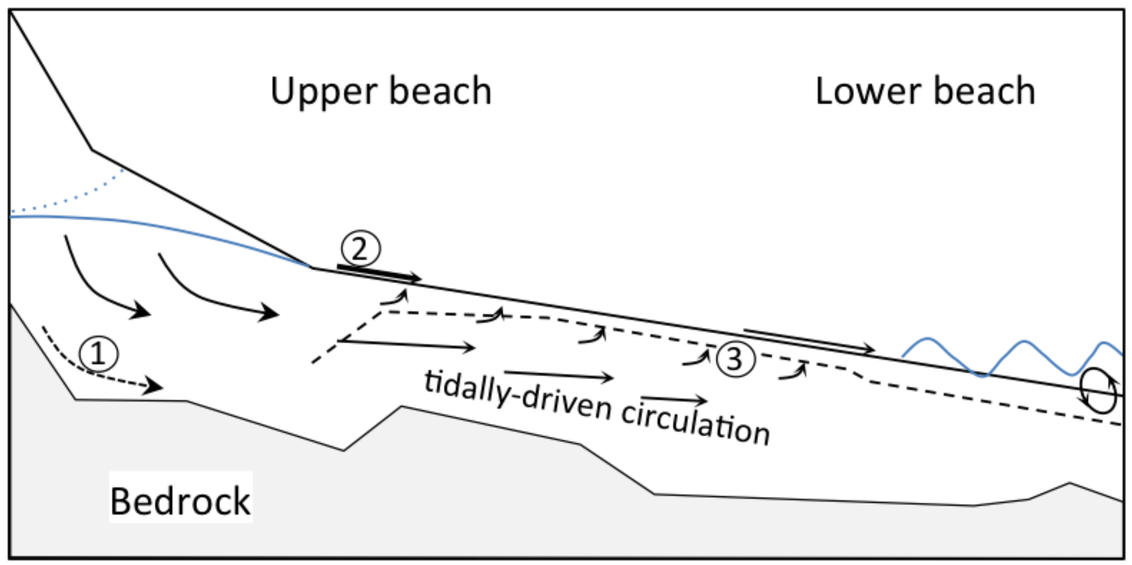
Upper beach
Lower beach
①
②
③
tidally-driven circulation
Bedrock

Table 1. Characteristics of sediments in the seepage zone of the Ker Chalon beach (mean ± standard deviation, N=6 for grain size and N=11 for other parameters)

| | |
|---|---|
| Median grain size (µm) | 166 ± 10 |
| Particulate organic carbon (% dry sediment) | 0.20 ± 0.08 |
| Particulate $CaCO_3$ (% dry sediment) | 18.2 ± 4.6 |
| HCl-extracted Fe (µmol $g^{-1}$) | 48.6 ± 3.5 |
| HCl-extracted Mn (µmol $g^{-1}$) | 1.21 ± 0.2 |
| HCl-extracted P (µmol $g^{-1}$) | 12.1 ± 2.8 |